

RESEARCH ARTICLE

Open Access



The SISHN2 transcription factor contributes to cuticle formation and epidermal patterning in tomato fruit

Cécile Bres^{1†}, Johann Petit^{1†}, Nicolas Reynoud², Lysiane Brocard³, Didier Marion², Marc Lahaye², Bénédicte Bakan² and Christophe Rothan^{1,4*}

Abstract

Tomato (*Solanum lycopersicum*) is an established model for studying plant cuticle because of its thick cuticle covering and embedding the epidermal cells of the fruit. In this study, we screened an EMS mutant collection of the miniature tomato cultivar Micro-Tom for fruit cracking mutants and found a mutant displaying a glossy fruit phenotype. By using an established mapping-by-sequencing strategy, we identified the causal mutation in the *SISHN2* transcription factor that is specifically expressed in outer epidermis of growing fruit. The point mutation in the *shn2* mutant introduces a K to N amino acid change in the highly conserved 'mm' domain of SHN proteins. The cuticle from *shn2* fruit showed a ~fivefold reduction in cutin while abundance and composition of waxes were barely affected. In addition to alterations in cuticle thickness and properties, epidermal patterning and polysaccharide composition of the cuticle were changed. RNAseq analysis further highlighted the altered expression of hundreds of genes in the fruit exocarp of *shn2*, including genes associated with cuticle and cell wall formation, hormone signaling and response, and transcriptional regulation. In conclusion, we showed that a point mutation in the transcriptional regulator *SISHN2* causes major changes in fruit cuticle formation and its coordination with epidermal patterning.

Keywords: Mutant, SHINE, Cuticle, Epidermis, Cell wall, Ethylene

Core

In this study, we isolated the causal mutation underlying a tomato fruit glossy mutant by using an established mapping-by-sequencing strategy. A point mutation in the *SISHN2* transcriptional regulator was found to cause major changes in tomato fruit cuticle composition, architecture and properties and in epidermal patterning. The coordination by *SISHN2* of the cutin and polysaccharides deposition in the fruit cuticle likely involves a cross-talk with various hormones, including ethylene.

Gene & Accession

SISHN1 SGN accession: *Solyc03g116610*, *SISHN2* SGN accession: *Solyc12g009490*, *SISHN2_X1* NCBI accession: XP_004251719, *SISHN2_X2* NCBI accession: XP_004251720, *SISHN3* SGN accession: *Solyc06g053240*.

Introduction

The plant cuticle is localized on the outer face of primary cell walls of epidermal cells of aerial plant organs where it serves as a protective barrier, notably by preventing water loss and resisting pathogen infection. In tomato fruit, which recently emerged as a model system for studying plant cuticle, the cuticle is thick and astomatous and influences commercially important traits such as visual appearance, susceptibility to fruit cracking and post-harvest shelf-life (Martin and Rose 2014; Petit et al. 2017).

[†]Cécile Bres and Johann Petit contributed equally to this work.

*Correspondence: christophe.rothan@inrae.fr

¹UMR 1332 BFP, INRAE, Université de Bordeaux, 33140 Villenave d'Ornon, France

Full list of author information is available at the end of the article



The cuticle is mainly composed of lipids, carbohydrates, and phenolics.

The surface of the fruit is covered by an epicuticular film of waxes. The wax fraction is typically a complex mixture composed of derivatives of very-long-chain fatty acids (VLCFA), mainly alkanes and alcohols, which may also include various secondary metabolites, such as amyryns, flavonoids and sterols. The synthesis of the aliphatic compounds involves several steps involving the synthesis of VLCFA through a multienzyme fatty acid elongase (FAE) complex and of VLCFA derivatives through either the alcohol forming pathway producing primary alcohols and wax esters, or the alkane forming pathway producing aldehydes, alkanes, secondary alcohols and ketones (Bernard and Joubès 2013). Export of waxes through plasma membrane occurs via ABC and LTPG transporters (Bernard and Joubès 2013).

The main component of the cuticle is cutin, which forms a continuum with the polysaccharides of the outer walls of epidermal cells. (Philippe et al. 2020a, 2020b). The cutin matrix is a polyester of polyhydroxy and epoxy fatty acids and fatty alcohols, with varying amounts of phenolic compounds (e.g. p-coumaric acid). In most plants, including tomato, the main cutin monomers are C16-based fatty acids (C16 dihydroxy fatty acids, C16 β -hydroxy fatty acids and C16 dicarboxylic acids) (Fich et al. 2016). The synthesis of cutin monomer starts with the synthesis of long chain fatty acids in the plastids. Fatty acids are transported to the cytoplasm where they undergo a series of modifications involving long-chain acyl-CoA synthetases (LACS), cytochrome P450-dependent fatty acid oxidases (CYP) and glycerol-3-phosphate acyl transferases (GPAT) to produce acyl-glycerols (Petit et al. 2016, 2017). Cutin precursors are then transferred via ABC transporters (Elejalde-Palmett et al. 2021) to the cell wall where they are assembled into a network of linear and branched cutin polymers (Philippe et al. 2016) by cutin synthases (Girard et al. 2012; Yeats et al. 2012; Fich et al. 2016).

In addition to the lipid polyesters, the roles of the polysaccharides and phenolic compounds in the structure and properties of the cuticle are increasingly being recognized (Philippe et al. 2020a, 2020b). The cuticle polysaccharides include pectins, which generally consist of polygalacturonans composed of the linear homogalacturonan (HG) and branched rhamnogalacturonan (RGI and RGII) (Atmodjo et al. 2013), hemicellulose that comprises xyloglucans and besides xylans and mananns (Lahaye et al. 2012), and cellulose (Jiang and Hsieh 2015). The cutin-embedded polysaccharides exhibit specific features including a high degree of esterification (i.e. methylation and acetylation) and a low ramification of the pectin RGI and a high crystallinity of cellulose (Philippe et al. 2020a).

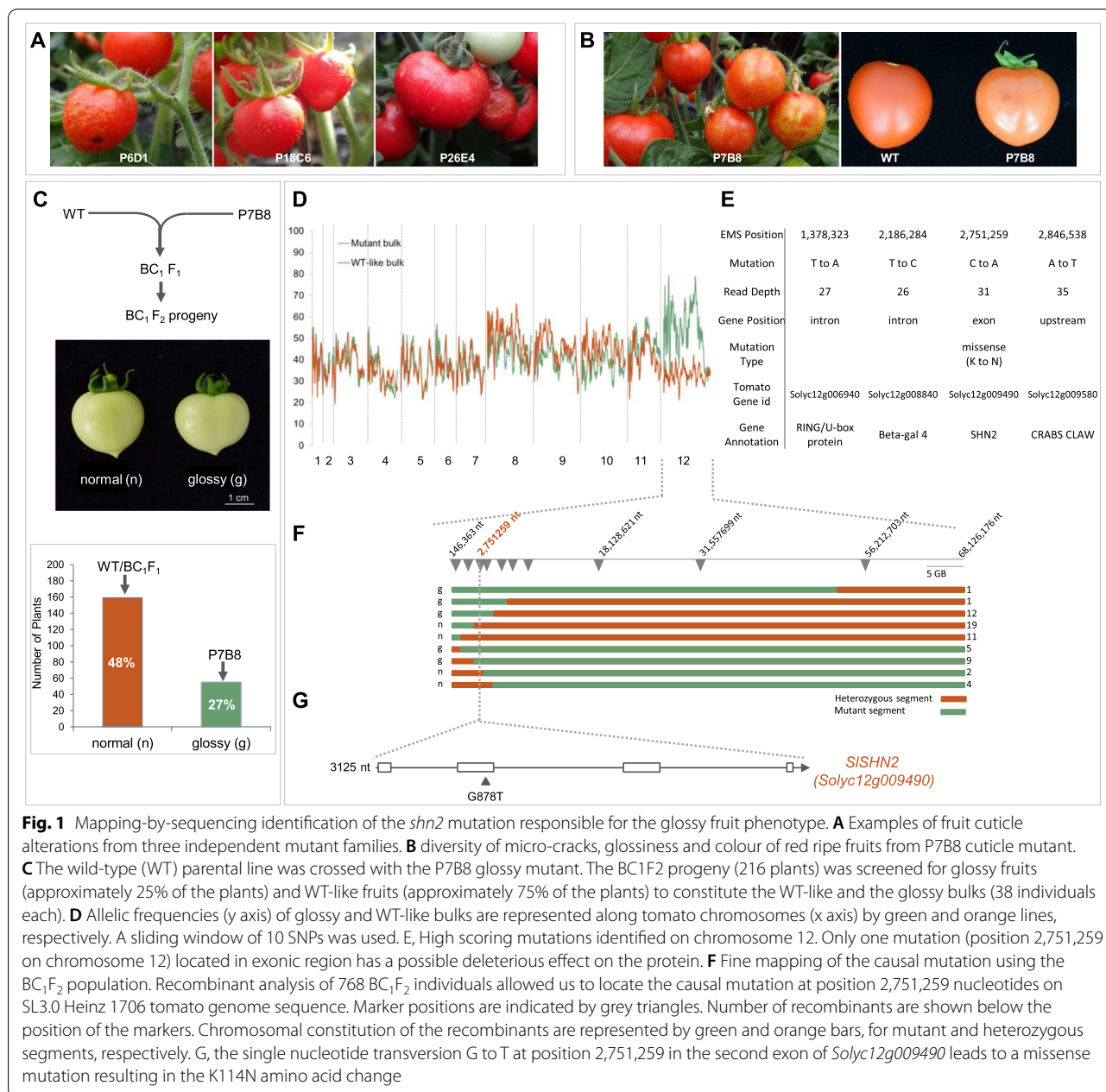
Together, cutin, cell wall polymers and phenolic compounds form the outer wall of the fruit and strongly contribute to the mechanical properties of the fruit skin (Philippe et al. 2020b; Khanal and Knoche 2017).

Here we used mapping-by-sequencing (MBS) to identify the causal mutation underlying a fruit cuticle mutant and established that a point mutation in the fruit-specific *SISHN2* transcription factor is responsible for increased fruit glossiness and cuticle defects in tomato. Functional characterization of the mutant further showed that *shn2* mutation alone is sufficient to alter fruit cutin and cutin-embedded polysaccharides content, composition, degrees of esterification and polymerization, cuticle properties and epidermal patterning of the fruit. Remarkably, mutation of *SHN2* affected the expression of hundreds of genes in the fruit exocarp, among which those associated with lipid polyester biosynthesis, phenylpropanoid pathway, cell wall synthesis and modification, and more unexpectedly, hormone synthesis and signaling (mainly ethylene, auxins and gibberellins).

Results

Identification of the causal mutation underlying a fruit glossy mutant via mapping-by-sequencing

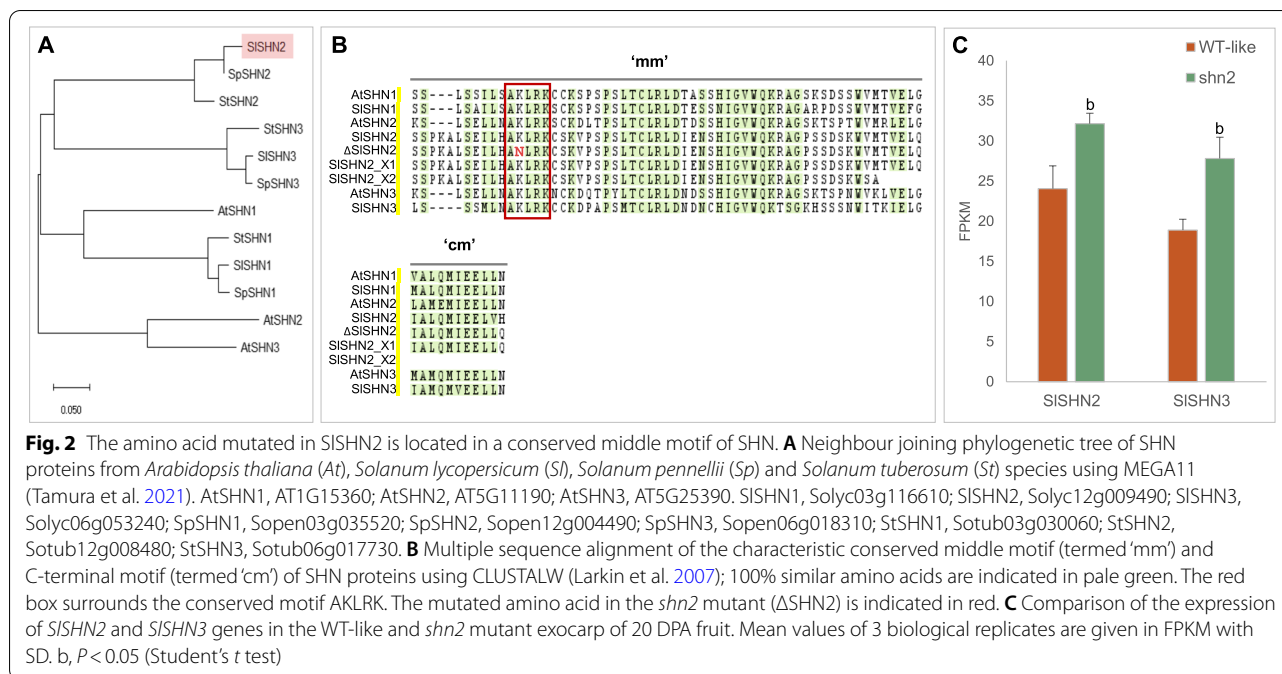
In previous studies, we isolated several *cutin-deficient* mutants (Shi et al. 2013; Petit et al. 2014, 2016) by screening an EMS-mutagenized tomato mutant population (Micro-Tom cultivar) (Just et al. 2013) for mutants showing increased fruit glossiness or colour changes. In the present study, we screened the same mutant population for mutants displaying more severe fruit surface defects including the presence of microcracks and evidences of wound-healing (Fig. 1A). We focused on one of these fruit surface mutants (line P7B8). The microcracks phenotype of P7B8 (Fig. 1B) was highly dependent on environmental conditions but consistently exhibited an enhanced fruit glossy phenotype (Fig. 1B). According to our previous study (Petit et al. 2014), this phenotype likely indicates a defect in cuticle formation and/or epidermal patterning. To facilitate identification of the mutant allele, we followed an established mapping-by-sequencing (MBS) strategy involving whole genome sequencing of bulked pools of individuals from a population segregating for the trait-of-interest (Garcia et al. 2016; Petit et al. 2016; Musseau et al., 2020). The homozygous P7B8 mutant line carrying a recessive *glossy* mutation was crossed with the WT (non-mutagenized) parental line in order to produce a BC₁F₁ hybrid plant, which was then selfed to generate a BC₁F₂ population (216 individuals). As the mutation underlying the microcracks/glossy phenotype is recessive, the BC₁F₂ population exhibited the expected



phenotypic ratio of 3:1 between "normal" and "glossy" fruit phenotypes (Fig. 1C). DNAs from pools of individuals showing either phenotype (38 individuals per pool) were submitted for whole genome sequencing (tomato genome coverage depth of 32X-33X; Supplemental Table S1A) and trimmed sequences were mapped onto the reference tomato genome (Tomato Genome Consortium, 2012; SL3.0 Heinz 1706) (Supplemental Table S1B) to detect allelic variants.

Analysis of the allelic variant frequencies in the two bulks led to the identification of chromosome 12 as the

genome region carrying the causal mutation, since it displayed low mutant allelic frequencies (AF < 0.4) in the WT-like bulk and much higher frequencies (AF > 0.95) in the glossy bulk (Fig. 1D and E and Supplemental Table S1C). Two chromosomal regions with high AF were detected on chromosome 12, which may be due to the presence of an unrelated introgression fragment from a wild tomato relative in the Micro-Tom cultivar, as described in Shirasawa et al. (2016). We therefore performed fine-mapping of the causal mutation using 768 BC₁F₂ individuals segregating for the glossy fruit



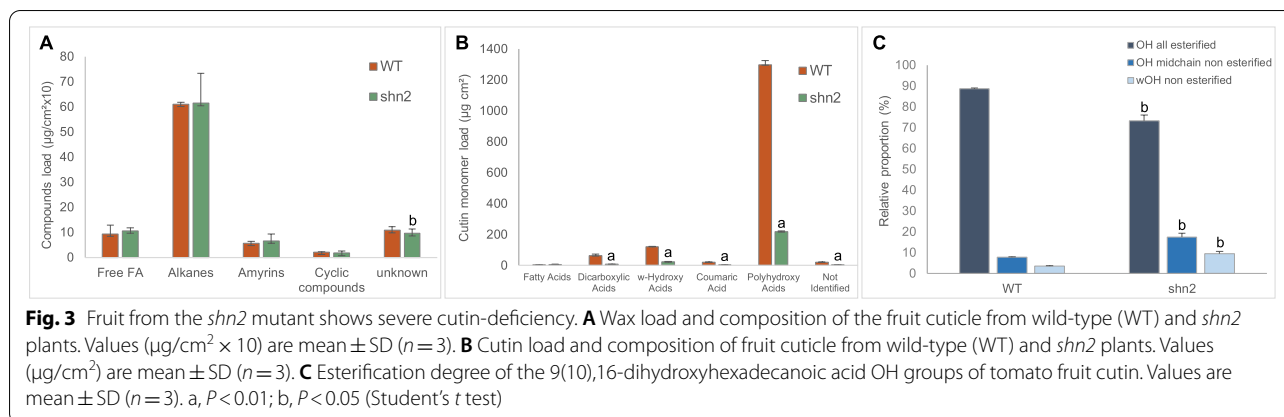
phenotype and EMS-induced SNPs in the regions of interest as genetic markers (Fig. 1F). Recombinant analysis allowed us to locate the causal mutation in a single chromosomal region with high AF (Fig. 1F). Analysis of the putative effects on protein functionality of the four high scoring mutations found in this region highlighted only one mutation located in exonic region that is predicted to affect protein structure (Fig. 1E). This mutation at position 2,751,259 on chromosome 12 (SL3.0 Heinz 1706 tomato genome sequence) was unequivocally associated to the glossy mutant trait as demonstrated by further recombinant analysis (Fig. 1F and G). The causal mutation affected a predicted AP2/ERF transcription factor previously annotated *SISHN2* (*Solyc12g009490*; Shi et al., 2013) (Fig. 1G). *SISHN2* belongs to the SHINE clade of proteins which have an established function in the regulation of cuticle formation and epidermal patterning (Aharoni et al., 2004; Shi et al., 2011, 2013).

The *shn2* mutation is located in the 'mm' conserved domain of SHN-like proteins

Three *SHN*-like genes have been identified in the tomato genome (Shi et al. 2013). *SISHN1* (*Solyc03g116610*) appears to be closest at the amino acid level to *A. thaliana* *AtWIN1/SHN1* (Al-Abdallat et al. 2014) whereas *SISHN3* (*Solyc06g053240*) is closest to *AtSHN3* (Shi et al. 2013). The *SISHN2* ortholog presents a lower homology with *A. thaliana* *SHN* proteins, ranging from 57 to 49% identity (66 to 63% similarity), and groups in a different cluster with other *SHN2*-like proteins from various Solanaceae

species including the wild tomato relative *Solanum pennellii* and the potato *Solanum tuberosum* (Fig. 2A). While *SISHN1* and *SISHN3* genes contain a single intron, as the *Arabidopsis SHN*-like genes, *SISHN2* contains a second intron. Furthermore, *SISHN2* has a predicted splice variant that contains a third intron due to the alternative splicing of the second exon, thus indicating the possible production of two *SISHN2* isoforms. In addition to the AP2 domain, the isoform X1 (XP_004251719.1) shares with all *SHNs* from *A. thaliana* and other Solanaceae species the conserved middle and C-terminal domains, which are referred to as the 'mm' and 'cm' domains, respectively, in (Aharoni et al. 2004; Shi et al. 2011, 2013). The predicted isoform X2 (XP_004251720.1) also shares the conserved 'mm' domain, which is encoded by its third exon. However X2 (155 aa) lacks the 'cm' domain (Fig. 2B) and is therefore much shorter than X1 (220 aa). Recombinant analysis (Fig. 1F and G) clearly indicated that the single G to T nucleotide transition at the end of the second exon of *SISHN2* is responsible for the glossy fruit phenotype of *shn2*. Specifically, the K114N mutation introduces a non-cationic amino acid change in the highly conserved cationic KLRK peptide motif of the 'mm' domain common to isoforms X1 and X2 (Fig. 2B).

In silico analysis of the expression of tomato *SHN*-like genes indicated that all three are weakly expressed in vegetative organs and predominantly expressed in reproductive organs (Shinozaki et al. 2018). *SISHN2* is highly expressed in the young growing fruit, like *SISHN3* which is also highly expressed in developing seeds



(Supplementary Figure S1A). *SISHN1* is highly expressed in unopened flower bud but not in the fruit. *SISHN2* transcripts are abundant in the fruit outer epidermis in a narrow time window spanning the cell expansion phase, before the onset of ripening, from 10 days post anthesis (DPA) to Mature Green stage (MG) (Supplementary Figure S1B). *SISHN3* shares a similar pattern of expression in the fruit, being expressed from 5 DPA to MG stage. In contrast to *SISHN2*, *SISHN3* is equally expressed in the outer and inner epidermis (Supplementary Figure S1A, B and C). The transcript abundance of *SISHN2* in fruit outer epidermis peaks at 20 DPA i.e. when fruit growth rate is maximum (Guillet et al. 2002) at which stage it is twice higher than that of *SISHN3* (Supplementary Figure S1B).

To analyze the expression of differentially expressed genes (DEGs), we performed RNAseq analysis of 20DPA fruit exocarp from *shn2* and WT. The WT control plants used for RNAseq analysis, named WT-like, are BC₁F₂ individuals which do not carry the *shn2* mutation. RNAseq analysis indicated that *SISHN2* and *SISHN3* were both detected in 20 DPA fruit exocarp (Fig. 2C) of WT and *shn2*. Interestingly, transcript abundances of *SISHN2* and *SISHN3* were higher in the *shn2* mutant (significant at $P < 0.05$ but not at $P < 0.01$) indicating that the *shn2* mutation has no deleterious effect on transcript stability of *SISHN2*. Mapping of the reads onto the tomato genome (ITAG3.2) confirmed the presence of *SISHN2* X1 and X2 transcripts variants (Supplementary Figure S2). Counting reads further indicated that the ratios of X1 and X2 transcripts are similar in *shn2* and WT. As expected, *SISHN1* was not detected.

Fruit from the *shn2* mutant shows severe cutin-deficiency

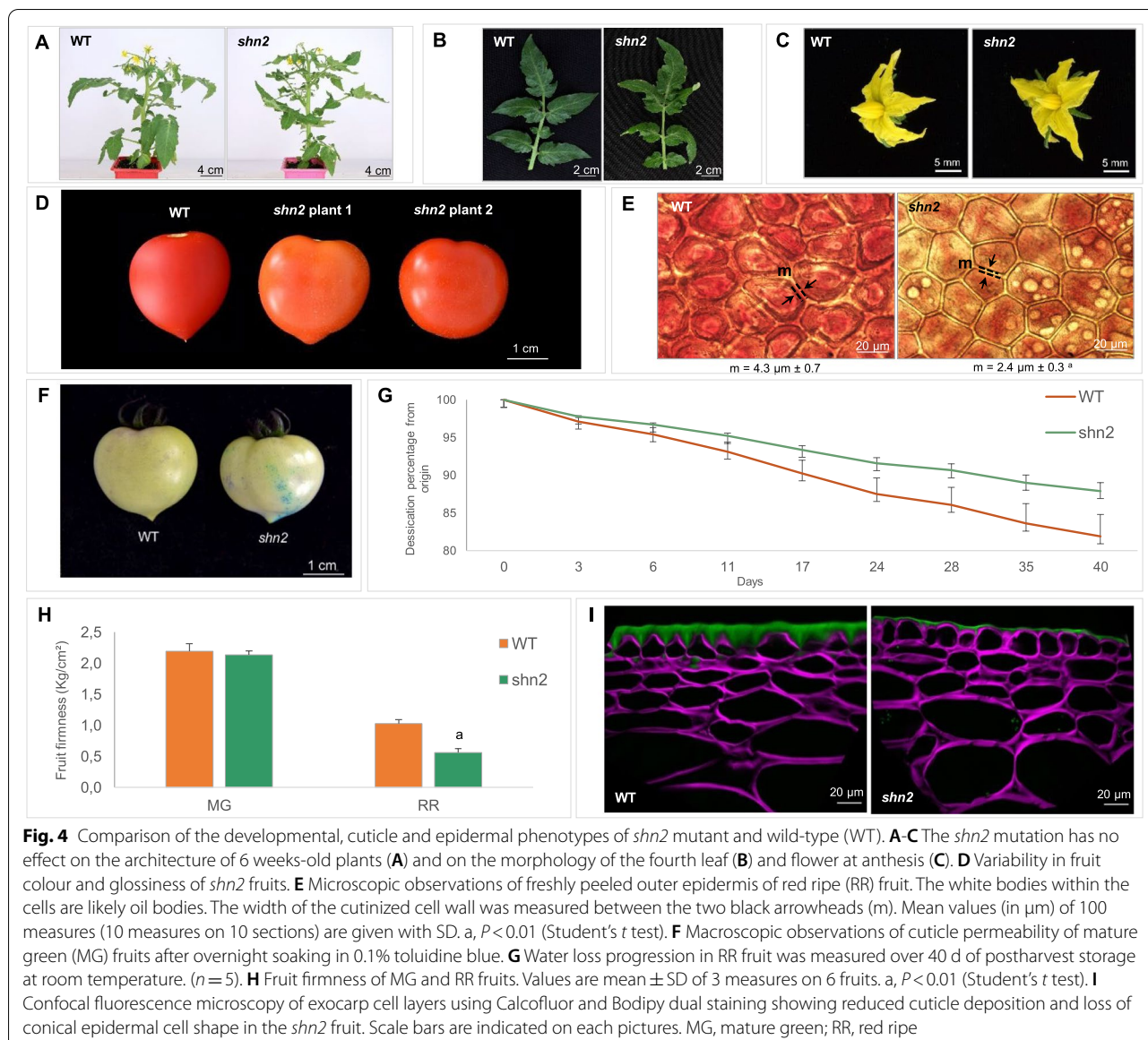
In order to investigate how the mutation in *SISHN2* gene affects cuticle composition, we analyzed the wax and cutin constituents of 20 DPA fruit cuticle. No differences

in wax loading were observed for the major classes of compounds between WT and *shn2* fruits (Fig. 3A). However, detailed analysis of wax compounds revealed differences in alkane composition (Supplementary Table S2), including decreased levels in C25, C27 (2.9-fold reduction) and increased levels in C33 (1.6-fold increase) alkanes in the *shn2* mutant. These variations were likely dependent on the decarboxylation pathway of alkane biosynthesis and not on the reductive pathway because only odd-numbered alkanes were significantly affected (Bernard and Joubès 2013).

In contrast to waxes, the total cutin load in *shn2* was reduced by 5.5-fold, from 1674 to 302 $\mu\text{g}/\text{cm}^2$ (Supplementary Table S3); this reduction affected all classes of compounds (Fig. 3B). This corresponded to a ~sixfold drop in the amount of the major cutin monomer 9(10), 16-dihydroxyhexadecanoic acid, a 7 to ~12-fold reduction of dicarboxylic acids C16:0 DCA and C16:0 DCA 9(10) OH and a 3.3 to 6.3-fold reduction of ω -hydroxy acids C16:0 ω OH, C16:0 ω OH 10-oxo, C18:0 ω OH (9 or 10) OH and C18:0 ω OH (9, 10) epoxy. Cutin reduction was not restricted to fatty acids-related monomers as the phenylalanine-derived *p*-coumaric acid was also severely reduced (tenfold reduction). As cuticle function is closely related to the structure of the cutin polymer, in which cutin polymerization plays a key role, we further checked the esterification degree of the OH groups from 9(10), 16-dihydroxyhexadecanoic acid using an established technology (Philippe et al. 2016). All esterified OH were significantly reduced in *shn2* while midchain and ω non-esterified OH were increased by more than two-fold (Fig. 3C).

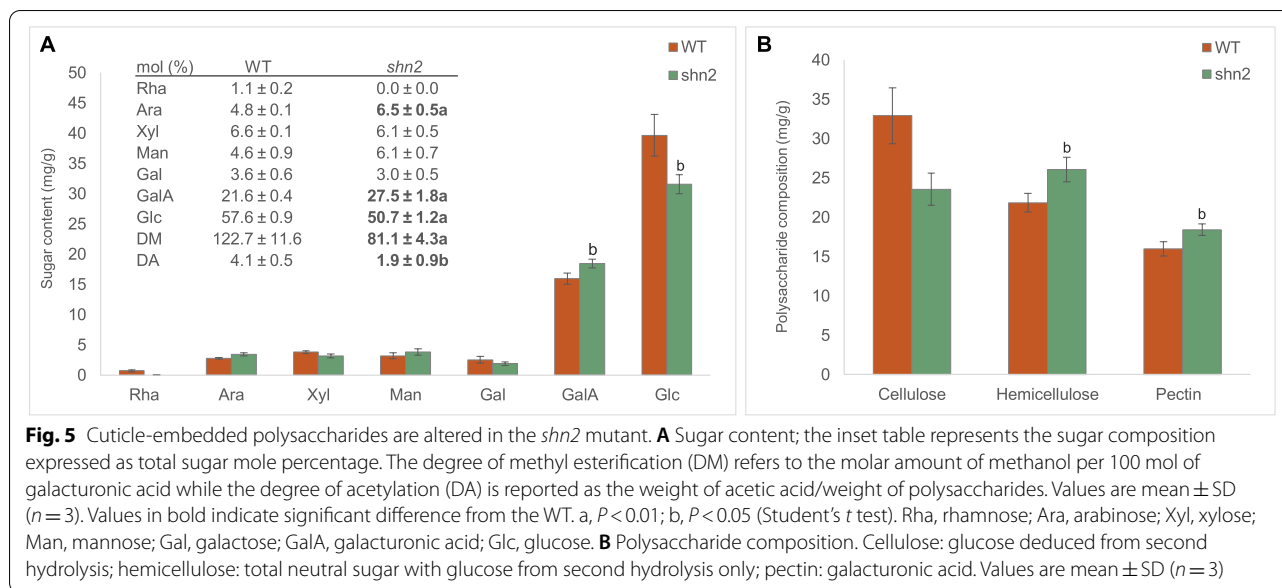
Cuticle thickness and properties are altered in the *shn2* mutant

Consistent with the strong and preferential expression of *SISHN2* in young developing fruit, whole plant, leaf



and flower phenotypes were identical in *shn2* and WT (Fig. 4A, B and C). Mutant fruits were consistently glossier and the ripe fruits had an orange hue (Fig. 4D). The expressivity of both traits was however variable (Fig. 4D) and *shn2* fruits were more or less glossy or orange according to environmental factors such as growth season and position of the plant in the greenhouse. In agreement with the strongly reduced cutin content (Supplementary Table S3), the most striking effect of the *shn2* mutation was on the fruit cuticle. The width of the anticlinal cutinized cell wall between adjacent epidermal cells was substantially reduced, by almost two-fold, in the *shn2* mutant (Fig. 4E). In addition, depending on the environmental conditions, subcellular structures reminiscent of

oil bodies could be observed in epidermal cells of ripe *shn2* mutant fruits (Fig. 4E). These profound changes in fruit cuticle led to modifications in fruit cuticle permeability as measured by toluidine blue staining (Fig. 4F). Unexpectedly, water loss was not increased but greatly reduced in *shn2* (Fig. 4G). Moreover, fruit firmness measured at red ripe stage with a penetrometer was also significantly reduced in *shn2* (Fig. 4H). As this may result from alterations in cuticle properties and epidermal cell features, we further analyzed the characteristics of epidermal and sub-epidermal cells of 20 DPA tomato fruit by BODIPY staining of neutral lipids and Calcofluor-white staining of cellulose (Fig. 4I). The results revealed a considerably thinner cuticle in *shn2* than in WT, the



absence of cuticular anticlinal pegs between epidermis cells and the lack of cutinization of sub-epidermal cell layers in *shn2*. Moreover, we observed that epidermal cells from *shn2* did not display the characteristic cone-shaped morphology of WT cells but were round-shaped with more intense staining of epidermal cell walls. No obvious variations in cell size or morphology were observed in sub-epidermal cells. The same observations were made in WT-like plants (Supplementary Figure S3) indicating that the phenotypic alterations observed were independent from other EMS mutations found in *shn2*. Taken together, these results indicate that the *shn2* mutation profoundly alters both cuticle deposition and epidermal patterning.

Composition of cutin-embedded polysaccharides is significantly altered in the *shn2* mutant

To further investigate the impact of *shn2* mutation on epidermal patterning, we analyzed the composition of cutin-embedded polysaccharides (CEP) (Philippe et al. 2020a) (Fig. 5). Significant differences were observed between the *shn2* mutant and WT regarding the galacturonic acid content, which was 1.15-fold higher in *shn2*, and in glucose, which was 1.26-fold lower in *shn2* (Fig. 5A). Because variations in sugar composition likely reflect changes in the abundance of the various cell wall polymers, we next analyzed the composition of CEP (Fig. 5B). *shn2* displayed a significant decrease in cellulose (1.4-fold) and, in contrast, significant increases in both hemicellulose (1.19-fold) and pectin (1.15-fold). To get further insight into polysaccharide structure, we examined the molar ratios of the various sugars present

in CEP (Fig. 5A inset). The ratio of ((Ara + Gal)/Rha) is currently used to evaluate the extent of rhamnogalacturonan (RGI) branching while the ratio (uronic acid)/(rhamnose + arabinose + galactose) is used to evaluate the linearity of pectins embedded within the cutin layers (Houben et al. 2011; Philippe et al. 2020a). The ratio of (Xyl/Man) is used to evaluate the proportion of mannan to xyloglucane in the hemicellulose fraction. These ratios showed a higher branching level of RGI in WT fruit than in *shn2*, where rhamnose content was below the detection limit of the method. A higher proportion of mannan in the hemicellulose fraction of *shn2* was observed compared to WT. This was accompanied by a decrease in pectin methylesterification (X 1.5 fold) and a considerable decrease in the acetylation of CEP (X 2.2 fold) (Fig. 5A inset).

Analysis of differentially expressed genes in developing fruit exocarp of *shn2* and WT

Since the *shn2* mutation has a pleiotropic effect on fruit epidermis and affects not only cuticle formation but also epidermal cell wall and morphology, we further investigated gene expression changes in the fruit exocarp. The fruit exocarp is defined here as the tissue obtained during the peeling of the fruit; it is mostly constituted of epidermal cells and underlying cutinized sub-epidermal cells (Petit et al. 2016; Renaudin et al. 2017). The 20 DPA developmental stage was selected because it corresponds to the maximum rate of fruit growth (Guillet et al. 2002) and cuticle formation in Micro-Tom (Mintz-Oron et al. 2008; Petit et al. 2014), and to the peak of *SISHN2* expression in the fruit (Supplemental Figure

S1). In order to exclude any potential effect of additional EMS mutations carried by the P7B8 line on gene expression changes in the mutant and to take into account the variable expressivity of the *shn2* mutation, we constituted pools of exocarp *shn2* and WT-like samples as follows. After recombinant analysis, BC1F3 homozygous progenies for either the mutant allele (*'shn2/shn2'* genotype; hereafter referred to as *shn2*) or the WT allele (*'SHN2/SHN2'* genotype; hereafter referred to as WT-like) were used to collect 20 DPA fruit exocarp.

Transcripts expressed in the fruit exocarp were subjected to high-throughput RNA sequencing analysis (RNAseq) using Illumina technology. Among the ~21,891 genes detected, 1927 were found to be differentially expressed between WT-like and *shn2* fruit exocarp using a two-fold cut-off on fold change in transcript abundance (ratio of 1 and -1 on a log₂ scale) and a *q*-value < 0.05. Of these, 1433 genes and 494 genes were expressed at higher or lower levels, respectively, in *shn2* than in WT-like. We further restricted our analysis to the most highly expressed genes by using an additional cut-off on the normalized number of reads (FPKM > 5 in either the mutant or the WT-like). This stringent analysis selected 921 genes among which the majority (753) was expressed at higher levels while 168 DEGs were expressed at lower levels in the *shn2* mutant (Supplementary Figure S4A). A wide range of biological processes were identified within the DEGs by Gene Ontology (GO) term enrichment analysis (Supplementary Figure S4B). Several categories related to the phenotype-of-interest, including cuticle formation and regulation, cell wall synthesis and modification, regulation of developmental and defense processes, and hormone-associated processes were expressed at higher or lower levels in the *shn2* mutant. The largest categories comprised DEGs associated with the regulation of transcription (78 DEGs) (Supplemental Table S4) and DEGs related to plant defense. As expected, significant differences were observed for lipid-related genes including 29 DEGs associated with cuticle formation (Table 1). We also detected 50 DEGs possibly involved in cell wall formation and modifications (Table 1 and Supplemental Table S5), in agreement with previous studies of lines in which the expression of *SHINE* was altered (Shi et al. 2011, 2013) and of tomato *gpa6a* mutant (Petit et al. 2016). Notably, we observed a number of DEGs (58) involved in hormone biosynthesis, signaling and action (Table 2). Among these were 29 DEGs associated with the ethylene-activated signaling pathway, one of the biological process ranking amongst the top 10 gene ontology terms (Supplementary Figure S4B). Several DEGs likely associated with the control of epidermal differentiation and development were also detected (Supplemental Table S6).

Genes involved in cuticle formation

Of the 29 DEGs involved in cuticle formation, 4 genes were associated with wax biosynthesis, 12 with cutin biosynthesis and assembly, 5 with lipid transport and 10 with phenylpropanoid pathway (Table 1). All wax-related genes were expressed at lower levels in the *shn2* mutant, with the exception of *Solyc06g074390*. While the expression of the *KCS/CER6* gene (*KCS_23*; *Solyc05g013220.2*) encoding a β -ketoacyl-CoA synthase enzyme that catalyzes the first step in the multi-enzymatic fatty acid elongase complex generating very long chains (VLCs) C20-C36 acyl-CoAs was lower in *shn2*, the expression of the *FAR/CER4* gene (*FAR_1a*; *Solyc06g074390*) encoding a fatty acyl-CoA reductase enzyme involved in the reductive pathway producing even-numbered carbon primary alcohols from VLCs-acyl-coAs was higher. At the opposite, the expression of two genes from the decarboxylation pathway yielding odd-numbered alkanes from VLC acyl-coAs was lower in the *shn2* mutant. *CER3* (*Solyc03g117800*) likely catalyzes the conversion of VLC acyl-CoAs to intermediate VLC aldehydes, and in association with *CER1*, to VLC alkanes. The expression of *CER3* is also strongly reduced in the *SIMIXTA-like* RNAi lines (Lashbrooke et al. 2015). *MAH1* (*CYP96A15*, *Solyc10g080840*) is a midchain alkane hydroxylase responsible for the generation of secondary alcohols and ketones derivatives from alkanes (Bernard and Joubès 2013). The cutin-related genes displayed contrasted behaviors in the *shn2* mutant compared with the WT. Cutin biosynthesis genes expressed at lower levels in *shn2* encode enzymes known to be required for the production of the MAG cutin precursors in tomato. They include two cytochrome P450-dependent fatty acid oxidases (CYP) for fatty acid ω -hydroxylation (*CYP86A69*, *Solyc08g081220*; *CYP86A8-like*, *Solyc04g082380*) (Shi et al. 2013) and one glycerol-3-phosphate acyltransferase (*GPAT6*, *Solyc09g014350*) (Petit et al. 2016) (Table 1). Notably, both *CYP86A69* and *CYP86A8-like* have been demonstrated to be SISHN3 target genes (Shi et al. 2013). Five DEGs encoded nonspecific lipid transfer (nsLTP) protein, examples of which have been suggested to be involved in the transport of cuticle components across the apoplast, although this has yet to be conclusively demonstrated (Yeats and Rose 2008). All were expressed at higher levels excepted for the *Solyc05g015490* gene encoding LTPG1, which was expressed at lower level. LTPG1, which is a major nsLTP from tomato fruit cuticle and a known allergen (Le et al. 2006), is also expressed at lower level in *cus1* RNAi lines (Girard et al. 2012) and in *gpat6a* tomato mutant (Petit et al. 2016). Seven GDSL-lipase genes were oppositely expressed at lower levels (3 DEGs) or at higher levels (4 DEGs). The *Solyc10g076740* gene encoding the CUS1 enzyme that catalyzes the

Table 1 Differentially expressed genes (DEGs) associated to cuticle modifications and cell wall polysaccharides

Category	Gene Identification	Putative Function	Log2 Fold Change <i>shn2</i> /WT	q value	
Wax Biosynthesis	Solyc05g013220	Ketoacyl-CoA synthase KCS	-1.97	5.0E-62	
	Solyc06g074390	Fatty acyl-CoA reductase FAR1	1.24	3.5E-17	
	Solyc03g117800	ECERIFERUM 3 CER3	-1.28	6.4E-58	
Cutin Biosynthesis	Solyc10g080840	Cytochrome P450 MAH1	-1.86	8.6E-209	
	Solyc08g081220	Cytochrome P450 CYP86A69 CD3	-2.20	1.3E-254	
	Solyc04g082380	Cytochrome P450 CYP86A8-like	-1.10	4.4E-08	
Lipid Transport	Solyc09g014350	Glycerol-3-phosphate acyltransferase GPAT6	-1.20	8.9E-69	
	Solyc10g075100	Non-specific lipid-transfer protein LTP2_1e	2.98	0.0E+00	
	Solyc09g018010	Non-specific lipid-transfer protein LTP2_2	1.37	6.9E-16	
Polymerization	Solyc10g075110	Non-specific lipid-transfer protein LTP2_1f	2.50	8.4E-31	
	Solyc08g067540	Non-specific lipid-transfer protein	1.57	3.4E-07	
	Solyc05g015490	Plant lipid transfer protein LTPG1	-3.37	7.0E-88	
	Solyc02g071610	GDSL esterase/lipase	1.58	7.3E-93	
	Solyc02g071700	GDSL esterase/lipase	2.41	2.1E-50	
	Solyc07g049440	GDSL esterase/lipase	-1.88	0.0E+00	
	Solyc03g121180	GDSL esterase/lipase	1.08	6.8E-74	
Regulation	Solyc10g076740	GDSL esterase/lipase CPRD49	-1.10	8.9E-29	
	Solyc11g006250	GDSL esterase/lipase CUS1	1.22	1.4E-69	
	Solyc06g083650	GDSL esterase/lipase CUS4	-1.12	1.1E-33	
	Solyc08g008610	Alpha/beta-Hydrolases superfamily protein BDG1	3.53	7.1E-151	
	Solyc02g088190	SIMIXTA-like	-1.08	1.0E-59	
	Phenylpropanoid Pathway	Solyc05g056170	Phenylalanine ammonia-lyase	-1.84	1.6E-122
		Solyc09g007890	Phenylalanine ammonia-lyase	1.17	4.8E-87
		Solyc10g086180	Phenylalanine ammonia-lyase	1.57	3.3E-42
		Solyc09g007910	Phenylalanine ammonia-lyase	2.47	2.8E-202
		Solyc00g500353	Phenylalanine ammonia-lyase	4.59	0.0E+00
Solyc09g007920		Phenylalanine ammonia-lyase	1.08	7.8E-84	
Solyc02g093230		Caffeoyl-CoA O-methyltransferase	1.78	9.9E-34	
Solyc02g093250		Caffeoyl-CoA O-methyltransferase	1.79	2.9E-50	
Solyc09g091510		Chalcone synthase 1 CHS1	1.91	6.6E-121	
Solyc01g111070		Chalcone synthase-like	1.32	3.6E-30	

Table 1 (continued)

Category	Gene Identification	Putative Function	Log2 Fold Change <i>shn2</i> /WT	q value
Cell Wall	Solyc12g015770	Cellulose synthase	-2.00	3.7E-83
	Solyc07g043390	Cellulose synthase	1.67	5.3E-41
	Solyc03g097050	Cellulose synthase	3.96	0.0E+00
	Solyc02g089640	Cellulose-synthase-like C4	1.71	1.8E-189
	Solyc01g065530	COBRA-like protein	1.92	2.2E-221
	Solyc08g081620	Endo-1,4-beta-glucanase precursor	-1.05	1.9E-07
	Solyc08g082250	Endo-beta-1,4-D-glucanase Cel8	1.01	7.5E-88
	Solyc07g049300	Endoglucanase	1.18	1.5E-61
	Solyc07g064870	Endoglucanase	1.59	5.1E-71
	Solyc03g071570	Pectate lyase	1.29	3.0E-60
	Solyc09g091430	Pectate lyase	1.90	9.2E-102
	Solyc09g061890	Pectate lyase	2.26	5.4E-231
	Solyc04g082140	Pectinesterase	1.31	4.6E-116
	Solyc06g009190	Pectinesterase	1.20	7.4E-36
	Solyc03g123620	Pectinesterase	2.71	0.0E+00
	Solyc03g083730	Plant invertase/pectin methylesterase inhibitor	1.65	2.8E-12
	Solyc12g010540	UDP-glucuronate 4-epimerase 4	1.70	3.9E-135
	Solyc05g051260	1,4-beta-xylanase	2.40	8.5E-07
	Solyc03g093080	Xyloglucan endotransglucosylase/hydrolase	3.50	0.0E+00
	Solyc07g055990	Xyloglucan endotransglucosylase/hydrolase	4.05	4.4E-208
	Solyc02g080160	Xyloglucan endotransglucosylase/hydrolase	1.62	3.6E-101
	Solyc07g056000	Xyloglucan endotransglucosylase/hydrolase	3.09	0.0E+00
	Solyc03g093110	Xyloglucan endotransglucosylase/hydrolase	3.96	0.0E+00
	Solyc07g009380	Xyloglucan endotransglucosylase-hydrolase 2	-1.14	3.0E-86
	Solyc03g093130	Xyloglucan endotransglucosylase-hydrolase 3	4.19	0.0E+00
	Solyc12g011030	Xyloglucan endotransglucosylase-hydrolase 9	3.02	5.7E-234
	Solyc12g017240	Xyloglucan endo-transglycosylase B1	2.73	0.0E+00
	Solyc07g044960	Xyloglucan galactosyltransferase KATAMARI1	3.89	6.7E-72
	Solyc03g093120	Xyloglucan:xyloglucosyl transferase TCH4	4.87	0.0E+00
	Solyc06g074670	UDP-apiiose/UDP-xylose synthase	2.57	0.0E+00

DEGs in the exocarp of WT-like and *shn2* 20 DPA fruit. Genes were assigned manually to functional categories. Annotations are from SGN

extracellular polymerization of cutin (Girard et al., 2012; Yeats et al., 2012) and is associated with the growth of the outer epidermal wall (Segado et al. 2020) was expressed at higher level, in contrast to its fate in the *gpat6a* tomato mutant (Petit et al. 2016). In contrast, the gene encoding CUS4 (*Solyc06g083650*), which displays the same developmental pattern as CUS1 during early fruit development but is much less expressed (Segado et al. 2020),

was expressed at lower level in *shn2*. The α/β -hydrolase BODYGUARD1 (*BDG1*; *Solyc08g008610*) is orthologous to the Arabidopsis AtBDG that was shown to be required for cutin biosynthesis, possibly through cutin polymerization (Jakobson et al. 2016). At last, a *SIMIXTA-like* gene (*Solyc02g088190*) encoding a MYB transcription factor at the core of the regulation of cutin biosynthesis in land plants (Xu et al. 2020) was expressed at lower

Table 2 Differentially expressed genes (DEGs) associated to hormones

Category	Gene Identification	Putative Function	Log2 Fold Change <i>shn2</i> /WT	q value
Gibberellin	Solyc12g006460	GA ent-kaurenoate oxidase	4.26	2.5E-249
	Solyc07g056670	Gibberellin 2-oxidase	-3.52	4.2E-46
	Solyc09g074270	Gibberellin receptor	2.34	1.1E-87
	Solyc04g017720	Gibberellin regulated protein GASA6	-2.04	2.3E-17
	Solyc04g078195	Gibberellin-regulated protein	1.12	5.0E-84
Ethylene synthesis and signalling	Solyc07g049550	1-aminocyclopropane-1-carboxylate oxidase 2 ACO2	-3.35	3.8E-26
	Solyc07g026650	1-aminocyclopropane-1-carboxylate oxidase 5 ACO5	-1.47	2.3E-13
	Solyc02g091990	Aminocyclopropane-1-carboxylate synthase 3 ACS3	3.48	1.4E-74
	Solyc09g089610	Ethylene receptor-like protein ETR6	-1.81	5.3E-38
Ethylene response	Solyc10g006130	EAR motif SIERF36	1.30	3.1E-135
	Solyc05g052030	Ethylene response factor 4	-3.90	8.6E-42
	Solyc03g093610	Ethylene response factor A.2	2.42	3.0E-144
	Solyc04g014530	Ethylene response factor C.2	-1.08	7.0E-14
	Solyc02g077370	Ethylene response factor C.5	1.74	2.1E-29
	Solyc03g093560	Ethylene response factor C.6	2.32	2.5E-35
	Solyc01g108240	Ethylene response factor D.3	3.96	0.0E+00
	Solyc10g050970	Ethylene response factor D.4	4.26	0.0E+00
	Solyc07g053740	Ethylene response factor F.4	1.29	2.1E-20
	Solyc05g051200	Ethylene-responsive factor 1	-2.02	6.8E-31
	Solyc04g011440	Ethylene-responsive heat shock protein cognate 70	2.44	0.0E+00
	Solyc02g070040	Ethylene-responsive nuclear protein ERT2	4.10	3.8E-135
	Solyc08g080630	Ethylene-responsive proteinase inhibitor 1	-7.90	4.6E-25
	Solyc12g056980	Ethylene-responsive transcription factor	-1.18	4.6E-15
	Solyc11g012980	Ethylene-responsive transcription factor	1.52	1.2E-62
	Solyc06g035700	Ethylene-responsive transcription factor	3.60	5.2E-59
	Solyc11g042560	Ethylene-responsive transcription factor	5.27	3.6E-56
	Solyc08g082210	Ethylene-responsive transcription factor	-1.43	2.3E-43
	Solyc12g009240	Ethylene-responsive transcription factor	1.26	3.2E-107
	Solyc01g090560	Ethylene-responsive transcription factor	1.60	3.3E-30
	Solyc01g090340	Ethylene-responsive transcription factor 2	3.88	3.5E-77
	Solyc02g077840	Ethylene-responsive transcription factor 4	1.17	1.1E-18
	Solyc08g078190	Ethylene-responsive transcription factor 5	1.15	1.7E-32
	Solyc03g093550	Ethylene-responsive transcription factor 5	1.62	4.6E-72
	Solyc03g093540	Ethylene-responsive transcription factor 5	2.28	6.1E-12
	Solyc04g078640	Ethylene-responsive transcription factor RAP2-1	-1.85	8.0E-11
Auxin synthesis, transport and response	Solyc06g062920	Auxin-regulated dual specificity cytosolic kinase	2.57	4.1E-236
	Solyc03g120380	Auxin-regulated IAA19	1.51	2.0E-37
	Solyc06g008580	Auxin-regulated IAA22	1.69	2.4E-22
	Solyc08g021820	Auxin-regulated IAA29	-2.31	5.2E-31
	Solyc12g096570	Auxin-regulated organ size gene	-4.27	1.6E-31
	Solyc06g075690	Auxin-regulated protein AF416289	4.87	5.5E-203
	Solyc04g053010	Auxin-responsive protein SAUR65	1.56	3.4E-74
	Solyc01g099840	Dormancy/auxin associated protein	-1.15	1.3E-44
	Solyc10g079640	IAA-amino acid hydrolase ILR1-like 6	1.74	2.1E-76
	Solyc06g059730	PIN6	6.11	3.3E-51
	Solyc01g110920	Small auxin up-regulated RNA26	-1.06	2.0E-18
	Solyc04g081250	Small auxin up-regulated RNA51	-1.39	2.4E-17
Solyc04g081270	Small auxin up-regulated RNA52	-1.93	8.6E-24	

Table 2 (continued)

Category	Gene Identification	Putative Function	Log2 Fold Change <i>shn2</i> /WT	q value
Abscisic Acid	Solyc02g084850	Abscisic acid environmental stress-inducible protein TAS14	1.13	3.8E-08
	Solyc03g095780	Abscisic acid receptor PYL4-like	1.99	3.7E-48
	Solyc08g005610	Cytochrome P450 CYP707A ABA	3.18	4.3E-26
Brassinosteroid	Solyc02g071990	Brassinosteroid signaling positive regulator-related protein BES1/BZR1	1.20	1.9E-55
	Solyc07g062260	Brassinosteroid signaling positive regulator-related protein BES1/BZR1	1.55	6.4E-34
Cytokinin	Solyc11g069570	Cytokinin riboside 5'-monophosphate phosphoribohydrolase	1.26	8.0E-12
Jasmonate	Solyc09g061840	3-ketoacyl-CoA thiolase peroxisomal-like	1.02	2.8E-26
	Solyc07g006890	Cytochrome P450 CYP94B jasmonate	3.01	0.0E+00
	Solyc12g009220	Jasmonate ZIM-domain protein 1	6.33	2.1E-139
	Solyc07g042170	Jasmonate ZIM-domain protein 3	1.82	3.9E-187
	Solyc08g076930	Jasmonic acid 3	1.11	3.2E-76

DEGs in the exocarp of WT-like and *shn2* 20 DPA fruit. Genes were assigned manually to functional categories. Annotations are from SGN

level. Silencing of the epidermis-expressed *SLMIXTA-like* gene in tomato results in the alteration of flattening of fruit epidermal cells, reduction in cuticle thickness and reduced expression of numerous cutin biosynthesis and assembly genes (Lashbrooke et al. 2015), including the GDSL-lipase genes *Solyc07g049440* and *Solyc03g121180* which were also less expressed in *shn2*.

The RNAseq data also indicated that the phenylpropanoid and flavonoid biosynthetic pathways were altered in *shn2* (Table 1). In the phenylpropanoid core pathway, five phenylalanine ammonia-lyase (PAL) genes (*Solyc00g300353*, *Solyc09g007890*, *Solyc09g007910*, *Solyc09g007920* and *Solyc10g086180*) were expressed at higher levels in *shn2* while only one (*Solyc05g056170*) was expressed at lower level. PAL catalyzes a committed step in the phenylpropanoid pathway that leads, via the *p*-coumaric acid that accumulates in the cuticle during fruit ripening (Lara et al. 2015), to the synthesis of *p*-coumaroyl-CoA that is a precursor of caffeoyl-CoA. Two caffeoyl-CoA O-methyltransferases (CCOAMT, *Solyc02g093230* and *Solyc02g093250*) catalyzing the formation of feruloyl-CoA from caffeoyl-CoA were up-regulated in *shn2*. In the flavonoid biosynthetic pathway, transcripts levels of two chalcone synthases (CHS1, *Solyc09g091510* and CHS-like *Solyc01g111070*) were higher in *shn2*. CHS catalyzes a committed step in the flavonoid pathway and uses *p*-coumaroyl-CoA as substrate to synthesize naringenin chalcone which gives the naringenin compound that accumulates in tomato fruit cuticle (Adato et al. 2009). Notably, transient silencing of chalcone synthase in tomato fruit resulted in changes in epidermal cell size and morphology (España et al. 2014a).

Genes involved in cell wall formation

In addition to the cuticle-associated lipid pathways, the most striking gene expression changes were related to polysaccharide cell wall pathways. Three genes encoding cellulose synthases (*Solyc02g089640*, *Solyc03g097050* and *Solyc07g043390*), the catalytic moiety required for the synthesis of cellulose microfibrils, were expressed at much higher levels in the *shn2* mutant. In contrast, the expression of the *Solyc12g015770* cellulose synthase gene, which is highly expressed in developing fruit until ripening (Song et al. 2019), was reduced in *shn2*. Conversely, the expression of a COBRA-like gene (*SICOB1*, *Solyc01g065530*), which encodes a glycosylphosphatidylinositol (GPI) anchored protein regulating epidermal cell wall thickness and cellulose formation in tomato fruit (Cao et al. 2012; Niu et al. 2015), was higher in *shn2*. Interestingly, in rice, a COBRA-like protein modulates cellulose assembly by interacting with cellulose and affecting microfibril crystallinity (Liu et al. 2013). We also detected the altered expression of genes related to pectins and hemicelluloses, the matrix polysaccharides of the primary cell wall. Among the pectin-related genes were DEGs encoding three pectate lyases (*Solyc03g071570*, *Solyc09g091430* and *Solyc09g061890*), three pectinesterases (*Solyc03g123620*, *Solyc04g082140* and *Solyc09g061890*) and one pectin methylesterase inhibitor (*Solyc03g083730*) that were expressed at higher levels in the *shn2* mutant. Together with the polygalacturonases, the pectate lyases may enable the incorporation of newly synthesized cell wall components during cell expansion. Pectinesterases and pectin methylesterase inhibitor may have opposite roles in controlling the esterification status

of pectins, which is thought to influence the mechanical properties of cell wall (Reca et al., 2012; Müller et al., 2013). The hemicellulose xyloglucan plays a key role in the loosening and tightening of cellulose microfibrils. The expression levels of 10 xyloglucan endotransglucosylase/hydrolase (XTH) genes were substantially higher in *shn2* mutant, with the exception of that of *Solyc07g009380*, which was reduced. XTH enzymes are involved in the integration of newly synthesized xyloglucans in the cell wall and therefore in assembly and restructuring of cell walls during cell expansion (Rose et al. 2002; Cosgrove 2005; Park and Cosgrove 2015).

Two genes encoding β -galactosidases (*Solyc06g062580* and *Solyc02g078950*), which may play roles in the modification of cell wall polysaccharides (Smith and Gross, 2000), were expressed at higher levels in the mutant while one β -glucosidase (*Solyc07g063390*) was expressed at lower level (Supplemental Table S5). In addition to the DEGs involved in the modification of cell wall polysaccharides, several DEGs encoded several proteins hypothesized to play central roles in cell expansion (Supplemental Table S5). Among them were expansins, which are important modulators of cell wall extensibility (Park and Cosgrove 2015). Three of them were expressed at much higher levels (*Solyc01g112000*, *Solyc05g007830* and *Solyc06g076220*) while one was expressed at lower level (*Solyc06g005560*). Four genes encoding arabinogalactan proteins also showed opposite patterns of relative transcript abundance in the *shn2* mutant and WT. Although the functions of arabinogalactan proteins are not well understood, they may play key roles in cell-wall architecture and composition (MacMillan et al. 2010). We also detected three DEGs encoding extensin-like proteins, which are hydroxyproline-rich glycoproteins essential for cell-wall assembly and growth by cell expansion, that were expressed at higher levels. Several other genes that may be involved in the coordination of epidermal cell wall development were also differentially expressed, including DEGs encoding EXORDIUM-like proteins (Sousa et al. 2020), Protodermal factor 1, and Long Cell-linked Cotton fiber protein (Supplemental Table S5).

Genes involved in transcriptional regulation

As could be expected, given the large transcriptional changes induced by the *shn2* mutation and the role of *SHN* genes in transcriptional regulation, the expression of 78 transcription factors (TFs) was altered, in addition to TFs involved in hormonal signaling. MYB (5), WRKY (15), AP2/B3 (2), bHLH (3), BZIP (3), GATA (2), GRAS (5), NAC (5), C2H2 zinc finger (13), Dof (2), LOB (3) and other TF categories (20) were expressed at higher (63) or lower (15) levels in *shn2* (Supplemental Table S5). All WRKY genes, which are well-known TFs regulating plant

abiotic and biotic stress tolerance (Li et al. 2020a), were expressed at higher levels in the *shn2* mutant. In addition, Dehydration-responsive element-binding (DREB) proteins, which also play a critical role in abiotic stress tolerance in plants (Lata and Prasad 2011), were expressed at much higher levels in the *shn2* mutant. To our knowledge most of these TFs have not previously been associated with TFs regulating fruit epidermis patterning or cuticle deposition (Borisjuk et al. 2014; Hen-Avivi et al. 2014), except for the MIXTA-like MYB transcription factor (Lashbrooke et al. 2015) and for HD Zip IV HDG2, a GLABRA 2-like protein that is a regulator of epidermal cell fate determination (Shi et al. 2013). Notably, a DEG encoding a chromatin structure-remodeling complex protein BSH (*Solyc11g013410*), which is a member of a multiprotein machinery controlling DNA accessibility with roles in the regulation of developmental and hormonal signaling pathways (Sarnowska et al. 2016), was expressed at much lower levels in the *shn2* mutant (Supplemental Table S6).

Genes involved in hormonal signaling and regulation of plant development

In addition to the above-mentioned TFs, the expression of DEGs encoding TFs involved in signaling of various hormones (gibberellin, ethylene, auxin, abscisic acid, brassinosteroid, jasmonate) were altered (Table 2). Moreover, the expression of DEGs encoding enzymes involved in hormone (gibberellin, ethylene, auxin, abscisic acid, jasmonate) biosynthesis was also altered. Genes involved in ethylene biosynthetic and signaling pathways (26 DEGs) were by far the most affected. Ethylene is a central hormone that fulfils various roles in plant and fruit development, among which the coordination of fruit ripening in tomato (Fenn and Giovannoni 2021), and the response to biotic and abiotic stresses (Müller and Munné-Bosch 2015). ACC synthase (ACS) and 1-aminocyclopropane-1-carboxylate oxidase (ACO) catalyze committed steps in ethylene biosynthesis. The ethylene signaling and response pathway includes the ethylene receptor (ETR6 is down-regulated in *shn2*) and Ethylene Response Factors (ERFs), which belong to the transcription factor family APETALA2/ERF. ERF are well suited to mediate the diversity of ethylene responses and the interactions with other hormones and redox signaling (Müller and Munné-Bosch 2015; Liu et al. 2016). The expression of twenty-three (23) DEGs encoding ERFs, among which possible transcriptional activators or repressors (Liu et al. 2016), were altered in *shn2*. After ethylene, the largest categories of hormone-related DEGs were auxin (13 DEGs), gibberellins (5 DEGs) and jasmonate (5 DEGs). Auxin plays essential roles in many developmental processes among which cell wall modification during cell expansion (Majda

and Robert 2018). The DEG encoding an auxin-regulated ARGOS-type protein (*Solyc12g096570*) that controls cell proliferation (Hu et al. 2003) was expressed at a much lower level. The gibberellins also regulate major aspects of plant growth and development, among which cell expansion. Interestingly, a recent study in tomato that linked a fruit firmness locus to cuticle thickness and composition (Li et al. 2020b) identified *GA2-OXIDASE* as the underlying gene. The mechanism by which *GA2-oxidase*, an enzyme of gibberellin catabolism that is strongly down-regulated in *shn2*, regulates cuticle formation is unknown although RNAseq analyses indicate *SISHN3* as a possible target (Li et al. 2020b). Surprisingly, relatively few DEGs were related to abscisic acid, regardless of its major role in the regulation of cuticle formation for plant resistance to pathogens and limitation of water loss (Currevers et al. 2010; Martin et al. 2017; Liang et al. 2021).

Discussion

Considerable advances in our understanding of the formation and architecture of cuticle have been made in the recent years thanks to the use of natural or artificially-induced genetic diversity available in cultivated tomato and in related wild species (Petit et al. 2021). To better understand fruit cuticle formation, we previously screened an EMS-mutagenized mutant collection in the miniature cultivar Micro-Tom (Just et al. 2013) for *cutin-deficient* (*cd*) mutants exhibiting increased fruit glossiness (Petit et al. 2014). We next identified several causal mutations in cytochrome P450-dependent fatty acid oxidase (*SICYP86A69*), glycerol-3-phosphate dehydrogenase (*SIGPAT6*) and cutin synthase (*SICUS1*) genes (Shi et al. 2013; Petit et al. 2014, 2016). Another tomato mutant collection (M82 cultivar) screened by Isaacson et al. (2009) led to the identification of mutations in *SICYP86A69* (Shi et al. 2013), *SICUS1* (Yeats et al. 2012) and *cd2*, a gene encoding a HD Zip IV transcription factor. These cuticle mutants proved to be precious tools to explore cuticle synthesis, structure and properties (Chatterjee et al., 2016; Philippe et al. 2016, 2020a; Moreira et al. 2020; Bento et al. 2021) and interaction with pathogens (Isaacson et al. 2009; Buxdorf et al. 2014; Fawke et al. 2019).

Cuticle formation is highly regulated throughout plant development, including during fruit growth (España et al. 2014b; Fich et al. 2016), and in response to environmental cues such as drought (Bernard and Joubès 2013). Many transcription factors (TFs) belonging to several families (AP2/ERF, DREB/CBF, MYB, HD-Zip IV and WW domain proteins) regulate wax and cutin synthesis and deposition (Borisjuk et al., 2014; Hen-Avivi et al. 2014). In tomato, exploitation of natural and artificially-induced genetic diversity led to the identification of

several TFs including an HD ZipIV (*cd2*) controlling wax, cutin and flavonoid composition of fruit cuticle (Isaacson et al. 2009; Nadakuduti et al. 2012), another HD Zip IV that regulates cutin and wax content as well as trichome formation (Xiong et al. 2020) and a SIMYB12 transcription factor regulating fruit cuticle flavonoids (Adato et al. 2009). Here we show that a nonsynonymous mutation in *SISHN2*, a member of the SHINE (SHN) clade of AP2/ERF regulatory TFs (Aharoni et al. 2004), affects the content and/or composition of wax, cutin, and cutin-incorporated polysaccharides, as well as the morphology of fruit epidermal cells.

An intriguing question is that of the possible redundancy of *SISHN2* and *SISHN3*. The two genes display similar developmental patterns and spatial localizations in epidermal cells except for the much higher expression of *SISHN2* at 10 DPA and its restriction to the outer epidermis. However, silencing (RNAi) of *SISHN3* (Shi et al. 2013) resulted in much milder cutin alterations than those observed in *shn2*. Although the *shn2* mutation significantly altered the expression of the two genes, the increase in *SISHN3* transcript abundance in *shn2* is moderate, suggesting no gene compensation by *SISHN3*. Comparison with the Arabidopsis *SHN* loss-of-function lines (Shi et al. 2011; Oshima et al. 2013) further suggests that *shn2* is a loss-of-function mutation resulting from the single non synonymous amino acid change located in a highly conserved SHN motif of *SISHN2*. Because the mutation falls into the 'mm' domain common to the two *SISHN2* isoforms and does not alter the relative abundance of *SISHN2_X1* and *X2* transcript variants, it probably does not affect alternative splicing of *SISHN2*, which could play a role under adverse environmental conditions, as has been demonstrated for the tomato cuticle gene *CWP* (Chechanovsky et al. 2019).

Modifications of wax and cutin load and/or composition were amongst the most obvious biochemical alterations observed in *shn2*. The strong reduction in cutin load affected all the major fatty acids-related monomers, including the 9(10),16-dihydroxyhexadecanoic acid that was also dramatically reduced in petals of *SHN*-silenced Arabidopsis lines (Shi et al. 2011), as well as the phenylalanine-derived *p*-coumaric acid. In addition, esterification levels of 9(10),16-dihydroxyhexadecanoic acid were modified as in the *cus1* cutin synthase mutant (Philippe et al. 2016), except that the proportion of non-esterified primary OH groups were much increased and that of secondary OH groups less increased in *shn2* than in *cus1*, suggesting a different pattern of cutin cross-linking in these mutants. Another original feature of *shn2* cuticle is the striking reduction in cutin-embedded cellulose and concomitant increase in hemicellulose and pectin. Moreover, RGI branching, pectin methylesterification and

acetylation of CEP were all decreased in *shn2*. Considering the increasingly obvious role of polyester-bound phenolics and CEP in cuticle features (reviewed in Philippe et al. 2020b; Reynoud et al. 2021), it is likely that changes in fruit cuticle-related properties (glossiness, permeability, firmness) and epidermal cell morphology observed in *shn2* are not only due to the reduction in cuticle thickness but also to alterations in cuticle composition and architecture (España et al. 2014b; Philippe et al. 2020a). An intriguing finding is the increased resistance of *shn2* to water-loss, which is likely independent of cutin deficiency (Isaacson et al. 2009; Philippe et al. 2016) and of the small changes in wax composition observed (Leide et al. 2007). It could be related to possible alterations in the structure of the cutin-polysaccharide-phenolic continuum, which warrant further investigations.

To date, little is known about the coordination of plant growth with the synthesis and deposition of cuticle components. Tomato mutants affected in cutin biosynthesis and assembly (Shi et al. 2013; Petit et al. 2014, 2016) or in flavonoid biosynthesis (España et al. 2014a) present variations of epidermal cell morphology reminiscent of *shn2*, suggesting feed-back regulation of cuticle deposition and epidermal patterning through a common regulatory network. Several lines of evidence, including the results presented herein, indicate that SHN TFs orchestrate cuticle formation and epidermal patterning by coordinating the synthesis of cuticle polyesters with the synthesis and modification of cuticle polysaccharides. In Arabidopsis, simultaneous silencing of the three *SHN* genes revealed that they redundantly regulate elongation and decoration of flower epidermal cells, probably through the reduction in cutin load and the modification of the cell wall pectins (Shi et al. 2011). Regulation of cuticle polysaccharides by SHN is further supported by results from ectopic expression of *AtSHN2* in rice, which oppositely increased cellulose and decreased lignin contents (Ambavaram et al. 2011). Further studies indicate that SHN and MIXTA-like regulators act coordinately to regulate cuticle deposition and epidermis differentiation. Indeed, expression of a MYB106 (a MIXTA-like TF) chimeric repressor induced cuticle deficiencies and reduced cutin nanoridges in Arabidopsis flowers (Oshima et al. 2013) i.e. phenotypes similar to those obtained by triple knock-down of *SHN* genes (Shi et al. 2011) and expression of a SHN1 chimeric repressor. In tomato, overexpression of *SISHN1* affected leaf wax deposition and plant drought resistance (Al-Abdallat et al. 2014) while RNAi silencing of *SISHN3* modified wax and cutin synthesis, epidermal patterning and pathogen susceptibility (Shi et al. 2013). Similar traits were affected by silencing tomato *SMIXTA-like*, which was proposed to act downstream

of *SISHN3*, possibly with HD Zip IV TFs (Lashbrooke et al. 2015).

Consistent with the biochemical alterations observed in *shn2*, transcriptome analysis revealed a set of genes associated with cutin synthesis and assembly and with the phenylalanine-derived pathway. These genes are likely targets of SISHN2 as their functions overlap with those of *SHN* targets previously reported in Arabidopsis (Shi et al. 2011; Oshima et al. 2013) and *SISHN3* and *MIXTA*-like targets in tomato (Shi et al. 2013; Lashbrooke et al. 2015). Accordingly, *SMIXTA-like*, which is also a target of *SISHN3* (Shi et al. 2013), was down-regulated in *shn2*. In addition, the expression of numerous genes associated with cell wall synthesis and modifications were altered. Co-regulation of genes related to lipid polyesters and cuticle polysaccharides has been observed in several cutin biosynthesis mutants (Voisin et al. 2009; Petit et al. 2016), which is not surprising considering the tight interactions between cuticle components (Reynoud et al. 2021). Our results strongly suggest a central role for SISHN2 in the control of cuticle deposition and architecture through the coordinated regulation in the growing fruit of genes associated to cutin and polysaccharide deposition. An intriguing feature is that the expression of the majority of cell wall-related genes detected is increased in *shn2* while, at the opposite, ectopic expression of *AtSHN2* in rice increased the expression of cellulose and other cell wall biosynthesis pathway genes (Ambavaram et al. 2011). The other feature highlighted by transcriptome analysis of *shn2* is the considerable number of DEGs related to phytohormones biosynthesis and signaling pathways. Our results support the role of GA in cuticle deposition, already highlighted in previous studies on Arabidopsis petal development (Shi et al. 2011) and tomato fruit firmness (Li et al. 2020b). They further position SISHN2 in the regulation network upstream of epidermis-expressed GA 2-oxidase, which likely controls active GA levels in epidermal cells. Additionally, our findings suggest a central role for ethylene in SISHN2 coordination of cuticle deposition, epidermal patterning and defense against biotic and abiotic stresses.

Conclusion

Tomato fruit undergoes a considerable increase in size during the cell expansion phase (Lemaire-Chamley et al. 2005; Musseau et al. 2020), a process to which the fruit must continually adapt by adjusting the morphology of its epidermal cells and the architecture and properties of the cuticle. In this study, *SISHN2* emerged as a key regulatory gene in the genetic program determining the adaptation of fruit epidermal and sub-epidermal cells to fruit growth. Hormonal signaling cascades and possibly epigenetic control of gene expression are likely part of

the regulation network involving *SISHN2*. Future studies positioning *SISHN2* in the genetic network that controls early fruit development will provide insights into how cuticle component synthesis and epidermal patterning are coordinated with fruit growth processes.

Material and methods

Plant materials

The tomato (*Solanum lycopersicum*) *glossy* mutant line P7B8 was isolated from an EMS (ethyl methanesulfonate) mutant tomato collection generated in the miniature Micro-Tom cultivar at INRAE (Bordeaux, France), as previously described (Petit et al. 2014). Thirty M_2/M_3 mutant families were selected in silico by screening our phenotypic mutant database (Just et al. 2013) for fruit cracking mutants. Following observation of 12 plants per family, one of the individuals of the P7B8 family showing a glossy fruit phenotype was isolated, selfed, and a single individual of the offspring carrying the homozygous *glossy* mutation was isolated. The parental Micro-Tom line used for EMS mutagenesis (Just et al. 2013) was used as a control unless otherwise indicated. An additional control (WT-like) used for several experiments (e.g. RNA-seq analysis) was a pool of P7B8 recombinant individuals carrying the same set of mutations as the *shn2* mutant except for the *shn2* mutation. All plants were grown in greenhouse under the conditions described in Rothan et al. (2016). Fruit glossiness was measured at the mature green (MG) and Red Ripe (RR) stages; photographs were taken under standardized conditions as described in Petit et al. (2014).

Mapping-by-sequencing

MBS and recombination analysis were performed as previously described (Garcia et al. 2016; Petit et al. 2016). A mapping BC_1F_2 population of 216 plants was created by crossing the P7B8 mutant with a WT parental line and by selfing a single BC_1F_1 hybrid. Two bulks were then constituted by pooling 38 plants displaying a glossy fruit phenotype (glossy bulk) or 38 plants with a dull/moderate glossy phenotype (WT-like bulk). DNA extracted from each bulk was used for preparation of libraries that were sequenced using a HiSeq 2500 sequencer (Illumina, 100-bp paired-end run mode) at the INRA-GeT-PlaGe-GENOTOUL platform. Sequence analyses were performed as previously described by Garcia et al. (2016), using version SL3.0 of the reference tomato genome for read mapping (ftp://ftp.solgenomics.net/genomes/Solanum_lycopersicum/Heinz1706/assembly/build_3.0/). EMS variants with a read depth between 10 and 100 were considered for allelic frequency analysis. Recombinant BC_1F_2 individuals were detected using the EMS-induced

SNPs flanking the putative mutation as markers in a Kompetitive allele-specific PCR (KASP) assay (Smith and Maughan, 2015). Subsequent genotyping of the causal *shn2* mutation was done through Sanger sequencing of PCR products (SHNseqF1 AGCAGAAGAAGCAGCAAGAGCAT; SHNseqR1 GGGGATACTTGTGCA TTATCCAA). Filtered EMS mutations were annotated using snpEff version 4.1 (Cingolani et al 2012) from build release SL3.0 of the reference tomato genome.

SISHN2 Phylogenetic analysis

A. thaliana and *S. lycopersicum* databases (TAIR 2021 and SGN 2021 respectively) were searched for SHINE amino acid sequences. Neighbor-joining (NJ) tree was then constructed using MEGA 11.0 (Tamura et al. 2021) and CLUSTALW (Larkin et al. 2007) with default parameters settings.

Measurement of the properties of fruit cuticle

For measurements of cuticle permeability to stain, we used a protocol adapted from Tanaka et al. (2004). MG fruits collected from WT and *shn2* mutant plants were placed in 0.1% toluidine blue solution for 16 h. Staining of the fruit surface was then visually scored and photographs were taken. For water loss measurements, red ripe (RR) fruits were harvested from WT, WT-like and *shn2* plants (5 fruits from 3 plants). For fruit sealing, Patafix (UHU) was then applied on peduncles and fruits were stored at room temperature. Fruit fresh weight was recorded at time zero and each week, until 40 days. Water loss was calculated as a percentage of weight loss. Fruit firmness was assessed by penetrometry using a Fruit Texture Analyser (GüSS, South Africa) equipped with a 5-mm diameter probe as previously described (Musseau et al. 2020). A minimum of 6 fruits from 6 different plants were analyzed as biological replicates.

Microscopy analysis of fruit cuticle

For measurement of cuticle thickness between two adjacent epidermal cells, microscopic observations were made on freshly peeled outer epidermal tissue from WT and *shn2* red ripe stage fruits and the width of the cutinized cell wall between two adjacent epidermal cells was measured as previously described (Petit et al. 2016). For the evaluation of the extent of cell cutinisation and morphology, transverse fresh sections of fruit exocarp were obtained from 3 independent 20 DPA stage fruits from WT and *shn2* plants. The sections were sequentially stained with calcofluor white stain (Sigma-Aldrich) for cell walls and BODIPY 493/503 (Thermo Fisher Scientific) for cuticle lipids. The sections were submerged for 30 s in 0.05% calcofluor white stain and washed for 5 min with PBS two times. They were then stained with

BODIPY solution (1 µg BODIPY per mL of PBS) for 5 min and washed in 1 ml of PBS and washed again. The stained sections were mounted on a slide in fluorescence mounting medium (CITIFLUOR AF1, England) and observed by confocal microscopy (Zeiss LSM880, Germany). Images were acquired with Zen 2011 software. All these experiments were realized at the Bordeaux Imaging Center (<http://www.bic.u-bordeaux.fr/>). Observations were made on WT, *shn2* homozygous mutant (*shn2/shn2*) and WT-like (*SHN2/SHN2*) individuals from the mapping BC₁F₂ population detected by KASP assay. For each genotype, a minimum of three pericarp sections from three fruits from different plants grown side-by-side were observed.

Cutin and wax analysis

Cuticular waxes were extracted by fruit immersion for 30 s in 6 mL of chloroform containing 6 µg of docosane as an internal standard and subsequently analyzed as previously described (Petit et al. 2014). For the cutin monomer analysis, two 1 cm diameter discs were isolated from a RR fruit epidermal peel, carefully scratched with a scalpel blade to remove exocarp cells and incubated for 30 min in isopropanol at 85 °C. The cutin was then delipidated, depolymerized and analyzed as previously described (Petit et al. 2014). Quantitative measurements were performed by gas chromatography with a Hewlett-Packard 5890 series II gas chromatograph equipped with a flame ionization detector (Bourdenx et al. 2011).

Sugar analyses

Cutin samples were prepared from isolated fruit peels and treated with cellulase and pectinase, as previously described (Girard et al. 2012), followed by 70% ethanol treatment and extensive dewaxing with chloroform. Polysaccharides were hydrolyzed by a two-step hydrolysis protocol using inositol as internal standard, as previously described (Philippe et al. 2020a). The alditol acetates of noncellulosic sugars released after sulfuric acid hydrolysis (1 M, 2 h, 100 °C) were analyzed by gas chromatography. To measure cellulosic glucose, a pre-hydrolysis step was included (72% H₂SO₄ for 30 min at 25 °C). Alditol acetates were analyzed on a Perkin Elmer AutoSystem (Perkin Elmer, Courtaboeuf, France) mounted with an OV-225 capillary column (J&W Scientific, Folsom, CA, USA; length 30 m, internal diameter 0.32 mm, operating at 205 °C with H₂ as the carrier gas). The quantification of uronic acids was performed on diluted aliquots using the meta-hydroxydiphenyl colorimetric method (Blumenkrantz & Asboe-Hansen, 1973). Cellulose content was deduced from the glucose specifically released during the pre-hydrolysis step. Hemicellulose content was

deduced from the amount of total neutral sugars (except glucose) without the pre-hydrolysis step. Pectin content was evaluated from the amount of uronic acid.

After an alkaline hydrolysis, the content of methanol released from the methyl esters substituting pectins was determined with an alcohol oxidase (*P. pastoris*, Sigma-Aldrich) by the N-methylbenzothiazolinone-2-hydrazone method (Anthon and Barrett, 2004). The acetic acid released was measured with a specific enzymatic kit (K-ACET, Megazyme, Wicklow, Ireland). The degree of methyl esterification refers to the mole amount of methanol per 100 mol of uronic acid, while the degree of acetylation (that can be released from pectin and hemicelluloses) refers to the mass of acetic acid per mass of polysaccharides.

RNAseq analysis

Twelve 1 cm diameter discs of epidermal peels were isolated from six 20 DPA fruits collected from three independent WT and *shn2* mutant plants and carefully scratched with a scalpel blade, as above. Two disks per fruit were collected in distinct pools and three pools were made in order to obtain three biological replicates. Samples were ground in liquid nitrogen and stored at -80 °C until RNA extraction. RNA was extracted using the RNA purification from plant and Fungi Nucleospin kit (Macherey–Nagel, Bethlehem, PA, USA), by following the supplier's recommendations. Total RNA integrity and concentration were assessed using an Agilent 2100 Bioanalyzer with RNA Nano Chip (Agilent Technologies, Santa Clara, California, USA). Total RNA samples were sequenced at the BGI Tech Solutions (Hong Kong SAR, China) facility. Bioinformatic analysis was performed with the integrated web-based BGI tool 'Dr. Tom' (<https://www.bgi.com/global/dr-tom/>). The Filtered RNA-seq reads were aligned to the tomato reference genome sequence *S. lycopersicum* build release SL3.00 (Species: *Solanum lycopersicum_4081*; Source: NCBI; Reference Genome Version: GCF_000188115.4_SL3.0) using HiSAT. Bowtie2 was used to align the clean reads to the reference genes. Annotated transcripts were obtained using ITAG4.0 gene models. Volcano Plot representation was done using R software with the EnhancedVolcano package, using data with following specifications: $-1 < \log_2FC < 1$; FPKM > 5, q Value < 0.07. The gene ontology (GO) enrichment analysis was performed with BLAST2GO (2021), with default parameters.

Statistical analysis

When appropriate, a Student's *t* test was performed.

Abbreviations

SGN: Sol Genomics Network; TAIR: The Arabidopsis Information Resource.

Supplementary Information

The online version contains supplementary material available at <https://doi.org/10.1186/s43897-022-00035-y>.

Additional file 1: Supplemental Figure S1. Digital expression of tomato SISHN2 and SISHN3 genes during tomato fruit development. **Supplemental Figure S2.** Transcripts variants of SISHN2. **Supplemental Figure S3.** Developmental, cuticular and epidermal phenotypes of WT-like plants. **Supplemental Figure S4.** Distribution of down- and up-regulated genes in 20 DPA fruit exocarp of WT-like and *shn2*.

Additional file 2: Supplemental Table S1. Mapping-by-sequencing data. **Supplemental Table S2.** Wax composition of the fruit cuticles of wild-type (WT) and *shn2*. **Supplemental Table S3.** Cutin composition of the fruit cuticle of wild-type (WT) and *shn2*. **Supplemental Table S4.** DEGs involved in transcriptional regulation. **Supplemental Table S5.** DEGs with possible roles in cell wall modifications. **Supplemental Table S6.** DEGs associated with epidermal patterning and development.

Acknowledgements

The authors gratefully acknowledge Isabelle Atienza for taking care of the plants in the greenhouse and help of Frédéric Domergue for wax and cutin analyses. Lipid analyses were performed in the Metabolome facility of Bordeaux and fruit cytology analysis at the Bordeaux Imaging Center, member of the national infrastructure France Biolmaging.

Authors' contributions

C.R., J.P., C.B. and B.B. designed the research; C.B. and J.P. performed the mutant screening; C.B. performed mapping-by-sequencing; J.P. performed cutin and wax analysis; N.R. performed cutin esterification and cell wall analyses; L.B. and C.B. performed confocal analysis; J.P. performed all other research; C.B., J.P. and C.R. performed data analysis; C.R. wrote the original draft of the article; C.B. and J.P. contributed to the original draft of the article; N.R., M.L., D.M. and B.B. reviewed and edited the article. The author(s) read and approved the final manuscript.

Funding

This work was supported by Bioadapt (grant ANR-13-BSV7-0012) "Adaptom" project, INRAE (TRANSFORM department) and Région Pays de la Loire (Ph.D. grant for N.R.).

Availability of data and materials

The lists of DEGs, log₂ ratios and *q*-values for several categories of differentially expressed genes are available in Tables 1 and 2 and in Supplemental Information (Supplemental Tables S4, S5 and S6). The RNAseq data (FASTQ files) and seeds of *shn2* tomato mutant underlying this article will be shared upon request to the corresponding author.

Declarations**Ethics approval and consent to participate**

Not applicable.

Consent for publication

Not applicable.

Competing interests

The authors declare no conflicts of interest.

Author details

¹UMR 1332 BFP, INRAE, Université de Bordeaux, 33140 Villenave d'Ornon, France. ²Unité Biopolymères, Interactions, Assemblages, INRAE, BP71627, 44316 Nantes Cedex 3, France. ³Univ. Bordeaux, CNRS, INSERM, Bordeaux Imaging Center, BIC, UMS 3420, US 4, 33000 Bordeaux, France. ⁴INRA, UMR

1332 Biologie du Fruit Et Pathologie, 71 Av Edouard Bourlaux, 33140 Villenave d'Ornon, France.

Received: 3 December 2021 Accepted: 3 May 2022

Published online: 07 June 2022

References

- Adato A, Mandel T, Mintz-Oron S, Venger I, Levy D, Yativ M, et al. Fruit-surface flavonoid accumulation in tomato is controlled by a SIMYB12-regulated transcriptional network. *PLoS Genet.* 2009;5:e1000777. <https://doi.org/10.1371/journal.pgen.1000777>.
- Aharoni A, Dixit S, Jetter R, Thoenes E, van Arkel G, Pereira A. The SHINE clade of AP2 domain transcription factors activates wax biosynthesis, alters cuticle properties, and confers drought tolerance when overexpressed in Arabidopsis. *Plant Cell.* 2004;16:2463–80. <https://doi.org/10.1105/tpc.104.022897>.
- Al-Abdallat AM, Al-Debei HS, Ayad JY, Hasan S. Over-expression of SISHN1 gene improves drought tolerance by increasing cuticular wax accumulation in tomato. *Int J Mol Sci.* 2014;15:19499–515. <https://doi.org/10.3390/ijms151119499>.
- Ambavaram MM, Krishnan A, Trijatmiko KR, Pereira A. Coordinated activation of cellulose and repression of lignin biosynthesis pathways in rice. *Plant Physiol.* 2011;155:916–31. <https://doi.org/10.1104/pp.110.168641>.
- Anthon GE, Barrett DM. Comparison of three colorimetric reagents in the determination of methanol with alcohol oxidase. Application to the assay of pectin methylesterase. *J Agric Food Chem.* 2004;52:3749–53. <https://doi.org/10.1021/jf035284w>.
- Atmodjo MA, Hao Z, Mohnen D. Evolving views of pectin biosynthesis. *Annu Rev Plant Biol.* 2013;64:747–79. <https://doi.org/10.1146/annurev-arpla-nt-042811-105534>.
- Bento A, Moreira CJS, Correia VG, Rúben Rodrigues RE, Geneix N, Petit J, et al. Quantification of structure–property relationships for plant polyesters reveals suberin and cutin idiosyncrasies. *ACS Sustain Chem Eng.* 2021;9:15780–92. <https://doi.org/10.1021/acssuschemeng.1c04733>.
- Bernard A, Joubès J. Arabidopsis cuticular waxes: advances in synthesis, export and regulation. *Prog Lipid Res.* 2013;52:110–29. <https://doi.org/10.1016/j.plipres.2012.10.002>.
- Blumenkrantz N, Asboe-Hansen G. An improved method for the assay of hydroxylysine. *Anal Biochem.* 1973;56:10–5. [https://doi.org/10.1016/0003-2697\(73\)90163-2](https://doi.org/10.1016/0003-2697(73)90163-2).
- Borisyuk N, Hrmova M, Lopato S. Transcriptional regulation of cuticle biosynthesis. *Biotechnol Adv.* 2014;32:526–40. <https://doi.org/10.1016/j.biotechadv.2014.01.005>.
- Bourdenx B, Bernard A, Domergue F, Pascal S, Léger A, Roby D, et al. Overexpression of Arabidopsis ECERIFERUM1 promotes wax very-long-chain alkane biosynthesis and influences plant response to biotic and abiotic stresses. *Plant Physiol.* 2011;156:29–45. <https://doi.org/10.1104/pp.111.172320>.
- Buxdorf K, Rubinsky G, Barda O, Burdman S, Aharoni A, Levy M. The transcription factor SISHINE3 modulates defense responses in tomato plants. *Plant Mol Biol.* 2014;84:37–47. <https://doi.org/10.1007/s11103-013-0117-1>.
- Cao Y, Tang X, Giovannoni J, Xiao F, Liu Y. Functional characterization of a tomato COBRA-like gene functioning in fruit development and ripening. *BMC Plant Biol.* 2012;12:211. <https://doi.org/10.1186/1471-2229-12-211>.
- Chatterjee S, Matas AJ, Isaacson T, Kehlet C, Rose JK, Stark RE. Solid-State (13) C NMR delineates the architectural design of biopolymers in native and genetically altered tomato fruit cuticles. *Biomacromol.* 2016;17:215–24. <https://doi.org/10.1021/acs.biomac.5b01321>.
- Chechanovsky N, Hovav R, Frenkel R, Faigenboim A, Eselson Y, Petreikov M, et al. Low temperature upregulates cwp expression and modifies alternative splicing patterns, increasing the severity of cwp-induced tomato fruit cuticular microfissures. *Hort Res.* 2019;6:122. <https://doi.org/10.1038/s41438-019-0204-9>.
- Cingolani P, Platts A, Wang IL, Coon M, Nguyen T, Wang L, et al. A program for annotating and predicting the effects of single nucleotide polymorphisms, SnpEff: SNPs in the genome of *Drosophila melanogaster* strain w1118; iso-2; iso-3. *Fly (austin).* 2012;6:80–92. <https://doi.org/10.4161/fly.19695>.

- Cosgrove DJ. Growth of the plant cell wall. *Nat Rev Mol Cell Biol.* 2005;6:850–61. <https://doi.org/10.1038/nrm1746>.
- Curvers K, Seifi H, Mouille G, de Rycke R, Asselbergh B, Van Hecke A. Abscisic acid deficiency causes changes in cuticle permeability and pectin composition that influence tomato resistance to *Botrytis cinerea*. *Plant Physiol.* 2010;154:847–60. <https://doi.org/10.1104/pp.110.158972>.
- Elejalde-Palmett C, Martínez San Segundo I, Garroum I, Charrier L, De Bellis D, Mucciolo A, et al. ABCG transporters export cutin precursors for the formation of the plant cuticle. *Curr Biol.* 2021;31:2111–2123.e9. <https://doi.org/10.1016/j.cub.2021.02.056>.
- España L, Heredia-Guerrero A, Reina-Pinto JJ, Fernández-Muñoz R, Heredia A, Domínguez E. Transient silencing of CHALCONE SYNTHASE during fruit ripening modifies tomato epidermal cells and cuticle properties. *Plant Physiol.* 2014;166:1371–86. <https://doi.org/10.1104/pp.114.246405>.
- España L, Heredia-Guerrero JA, Segado P, Benítez JJ, Heredia A, Domínguez E. Biomechanical properties of the tomato (*Solanum lycopersicum*) fruit cuticle during development are modulated by changes in the relative amounts of its components. *New Phytol.* 2014;202:790–802. <https://doi.org/10.1111/nph.12727>.
- Fawke S, Torode TA, Gogleva A, Fich EA, Sørensen I, Yunusov T, et al. Glycerol-3-phosphate acyltransferase 6 controls filamentous pathogen interactions and cell wall properties of the tomato and *Nicotiana benthamiana* leaf epidermis. *New Phytol.* 2019;223:1547–59. <https://doi.org/10.1111/nph.15846>.
- Fenn MA, Giovannoni JJ. Phytohormones in fruit development and maturation. *Plant J.* 2021;105:446–58. <https://doi.org/10.1111/tpj.15112>.
- Fich EA, Segerson NA, Rose JKC. The plant polyester cutin: biosynthesis, structure, and biological roles. *Annu Rev Plant Biol.* 2016;67:207–33. <https://doi.org/10.1146/annurev-arplant-043015-111929>.
- García V, Bres C, Just D, Fernández L, Wong Jun Tai F, Mauxion JP, et al. Rapid identification of causal mutations in tomato EMS populations via mapping-by-sequencing. *Nat Protoc.* 2016;11:2401–18. <https://doi.org/10.1038/nprot.2016.143>.
- Girard A-L, Mounet F, Lemaire-Chamley M, Gaillard C, Elmorjani K, Vivancos J, et al. Tomato GDSL1 is required for cutin deposition in the fruit cuticle. *Plant Cell.* 2012;24:3119–34. <https://doi.org/10.1105/tpc.112.101055>.
- Guillet C, Just D, Bénard N, Destrac-Irvine A, Baldet P, Hernould M, Causse M, et al. A fruit-specific phospho enolpyruvate carboxylase is related to rapid growth of tomato fruit. *Planta.* 2002;214:717–26. <https://doi.org/10.1007/s00425-001-0687-z>.
- Hen-Avivi S, Lashbrooke J, Costa F, Aharoni A. Scratching the surface: genetic regulation of cuticle assembly in fleshy fruit. *J Exp Bot.* 2014;65:4653–64. <https://doi.org/10.1093/jxb/eru225>.
- Houben K, Jolie RP, Fraeye I, Van Loey AM, Hendrickx ME. Comparative study of the cell wall composition of broccoli, carrot, and tomato: structural characterization of the extractable pectins and hemicelluloses. *Carbohydr Res.* 2011;346:1105–11. <https://doi.org/10.1016/j.carres.2011.04.014>.
- Hu Y, Xie Q, Chua NH. The Arabidopsis auxin-inducible gene ARGOS controls lateral organ size. *Plant Cell.* 2003;15:1951–61. <https://doi.org/10.1105/tpc.013557>.
- Isaacson T, Kosma DK, Matas AJ, Buda GJ, He Y, Yu B, et al. Cutin deficiency in the tomato fruit cuticle consistently affects resistance to microbial infection and biomechanical properties, but not transpirational water loss. *Plant J.* 2009;60:363–77. <https://doi.org/10.1111/j.1365-313X.2009.03969.x>.
- Jakobson L, Lindgren LO, Verdier G, Laanemets K, Brosché M, Beisson F, Kollist H. BODYGUARD is required for the biosynthesis of cutin in Arabidopsis. *New Phytol.* 2016;211:614–26. <https://doi.org/10.1111/nph.13924>.
- Jiang F, Hsieh YL. Cellulose nanocrystal isolation from tomato peels and assembled nanofibers. *Carbohydr Polym.* 2015;122:60–8. <https://doi.org/10.1016/j.carbpol.2014.12.064>.
- Just D, García V, Fernández L, Bres C, Mauxion J-P, Petit J, et al. Micro-Tom mutants for functional analysis of target genes and discovery of new alleles in tomato. *Plant Biotechnol.* 2013;30:225–31. <https://doi.org/10.5511/plantbiotechnology.13.0622a>.
- Khanal BP, Knoche M. Mechanical properties of cuticles and their primary determinants. *J Exp Bot.* 2017;68:5351–67. <https://doi.org/10.1093/jxb/erx265>.
- Lahaye M, Quemener B, Causse M, Seymour GB. Hemicellulose fine structure is affected differently during ripening of tomato lines with contrasted texture. *Int J Biol Macromol.* 2012;51:462–70. <https://doi.org/10.1016/j.ijbiomac.2012.05.024>.
- Lara I, Belge B, Goulao LF. A focus on the biosynthesis and composition of cuticle in fruits. *J Agric Food Chem.* 2015;63:4005–19. <https://doi.org/10.1021/acs.jafc.5b00013>.
- Larkin MA, Blackshields G, Brown NP, Chenna R, McGettigan PA, McWilliam H, et al. Clustal W and Clustal X version 2.0. *Bioinformatics.* 2007;23:2947–8. <https://doi.org/10.1093/bioinformatics/btm404>.
- Lashbrooke J, Adato A, Lotan O, Alkan N, Tsimbalist T, Rechav K, et al. The tomato MIXTA-like transcription factor coordinates fruit epidermis conical cell development and cuticular lipid biosynthesis and assembly. *Plant Physiol.* 2015;169:2553–71. <https://doi.org/10.1104/pp.15.01145>.
- Lata C, Prasad M. Role of DREBs in regulation of abiotic stress responses in plants. *J Exp Bot.* 2011;62:4731–48. <https://doi.org/10.1093/jxb/err210>.
- Le LQ, Lorenz Y, Scheurer S, Fötisch K, Enrique E, Bartra J, et al. Design of tomato fruits with reduced allergenicity by dsRNAi-mediated inhibition of ns-LTP (Lyc e 3) expression. *Plant Biotechnol J.* 2006;4:231–42. <https://doi.org/10.1111/j.1467-7652.2005.00175.x>.
- Leide J, Hildebrandt U, Reussing K, Riederer M, Vogg G. The developmental pattern of tomato fruit wax accumulation and its impact on cuticular transpiration barrier properties: effects of a deficiency in a beta-ketoacyl-coenzyme A synthase (LeCER6). *Plant Physiol.* 2007;144:1667–79. <https://doi.org/10.1104/pp.107.099481>.
- Lemaire-Chamley M, Petit J, García V, Just D, Baldet P, Germain V, et al. Changes in transcriptional profiles are associated with early fruit tissue specialization in tomato. *Plant Physiol.* 2005;139:750–69. <https://doi.org/10.1104/pp.105.063719>.
- Li W, Pang S, Lu Z, Jin B. Function and mechanism of WRKY transcription factors in abiotic stress responses of plants. *Plants (basel).* 2020;9:1515. <https://doi.org/10.3390/plants9111515>.
- Li R, Sun S, Wang H, Wan K, Yu H, Zhou Z, et al. FIS1 encodes a GA2-oxidase that regulates fruit firmness in tomato. *Nat Commun.* 2020;11:5844. <https://doi.org/10.1038/s41467-020-19705-w>.
- Liang B, Sun Y, Wang J, Zheng Y, Zhang W, Xu Y, et al. Tomato protein phosphatase 2C influences the onset of fruit ripening and fruit glossiness. *J Exp Bot.* 2021;72:2403–18. <https://doi.org/10.1093/jxb/eraa593>.
- Liu L, Shang-Guan K, Zhang B, Liu X, Yan M, Zhang L, et al. Brittle Culm1, a COBRA-like protein, functions in cellulose assembly through binding cellulose microfibrils. *PLoS Genet.* 2013;9:e1003704. <https://doi.org/10.1371/journal.pgen.1003704>.
- Liu M, Lima Gomes B, Mila I, Purgatto E, Peres LE, Frasse P, et al. Comprehensive profiling of Ethylene Response Factors expression identifies ripening-associated ERF genes and their link to key regulators of fruit ripening in tomato (*Solanum lycopersicum*). *Plant Physiol.* 2016;170:1732–44. <https://doi.org/10.1104/pp.15.01859>.
- MacMillan CP, Mansfield SD, Stachurski ZH, Evans R, Southerton SG. Fasciclin-like arabinogalactan proteins: specialization for stem biomechanics and cell wall architecture in Arabidopsis and Eucalyptus. *Plant J.* 2010;62:689–703. <https://doi.org/10.1111/j.1365-313X.2010.04181.x>.
- Majda M, Robert S. The role of auxin in cell wall expansion. *Int J Mol Sci.* 2018;19:951. <https://doi.org/10.3390/ijms19040951>.
- Martin LB, Rose JKC. There's more than one way to skin a fruit: formation and functions of fruit cuticles. *J Exp Bot.* 2014;65:4639–51. <https://doi.org/10.1093/jxb/eru301>.
- Martin LBB, Romero P, Fich EA, Domozych DS, Rose JKC. Cuticle biosynthesis in tomato leaves is developmentally regulated by abscisic acid. *Plant Physiol.* 2017;174:1384–98. <https://doi.org/10.1104/pp.17.00387>.
- Mintz-Oron S, Mandel T, Rogachev I, Feldberg L, Lotan O, Yativ M, et al. Gene expression and metabolism in tomato fruit surface tissues. *Plant Physiol.* 2008;147:823–51. <https://doi.org/10.1104/pp.108.116004>.
- Moreira CJS, Bento A, Pais J, Petit J, Escórcio R, Correia VG, et al. An ionic liquid extraction that preserves the molecular structure of cutin shown by nuclear magnetic resonance. *Plant Physiol.* 2020;184:592–606. <https://doi.org/10.1104/pp.20.01049>.
- Müller M, Munné-Bosch S. Ethylene response factors: a key regulatory hub in hormone and stress signaling. *Plant Physiol.* 2015;169:32–41. <https://doi.org/10.1104/pp.15.00667>.
- Müller K, Levesque-Tremblay G, Fernandes A, Wormit A, Bartels S, Usadel B, Kermode A. Overexpression of a pectin methylesterase inhibitor in Arabidopsis thaliana leads to altered growth morphology of the stem and

- defective organ separation. *Plant Signal Behav.* 2013;8:e26464. <https://doi.org/10.4161/psb.26464>.
- Musseau C, Jorly J, Gadin S, Sørensen I, Deborde C, Bernillon S, et al. The tomato guanylate-binding protein SLGBP1 enables fruit tissue differentiation by maintaining endopolyploid cells in a non-proliferative state. *Plant Cell.* 2020;32:3188–205. <https://doi.org/10.1105/tpc.20.00245>.
- Nadakuduti SS, Pollard M, Kosma DK, Allen C Jr, Ohlrogge JB, Barry CS. Pleiotropic phenotypes of the sticky peel mutant provide new insight into the role of CUTIN DEFICIENT2 in epidermal cell function in tomato. *Plant Physiol.* 2012;159:945–60. <https://doi.org/10.1104/pp.112.198374>.
- Niu E, Shang X, Cheng C, Bao J, Zeng Y, Cai C, et al. Comprehensive analysis of the COBRA-like (COBL) gene family in *Gossypium* identifies two COBLs potentially associated with fiber quality. *PLoS One.* 2015;10:e0145725. <https://doi.org/10.1371/journal.pone.0145725>.
- Oshima Y, Shikata M, Koyama T, Ohtsubo N, Mitsuda N, Ohme-Takagi M. MIXTA-like transcription factors and WAX INDUCER1/SHINE1 coordinately regulate cuticle development in *Arabidopsis* and *Torenia* fourieri. *Plant Cell.* 2013;25:1609–24. <https://doi.org/10.1105/tpc.113.110783>.
- Park YB, Cosgrove DJ. Xyloglucan and its interactions with other components of the growing cell wall. *Plant Cell Physiol.* 2015;56:180–94. <https://doi.org/10.1093/pccp/pcu204>.
- Petit J, Bres C, Just D, Garcia V, Mauxion J-P, Marion D, et al. Analyses of tomato fruit glossiness mutants uncover both cutin-deficient and cutin-abundant mutants and a new hypomorphic allele of GDLS lipase. *Plant Physiol.* 2014;164:888–906. <https://doi.org/10.1104/pp.113.232645>.
- Petit J, Bres C, Mauxion JP, Tai FW, Martin LB, Fich EA, et al. The glycerol-3-phosphate acyltransferase GPAT6 from tomato plays a central role in fruit cutin biosynthesis. *Plant Physiol.* 2016;171:894–913. <https://doi.org/10.1104/pp.16.00409>.
- Petit J, Bres C, Mauxion JP, Bakan B, Rothan C. Breeding for cuticle-associated traits in crop species: traits, targets, and strategies. *J Exp Bot.* 2017;68:5369–87. <https://doi.org/10.1093/jxb/erx341>.
- Petit J, Bres C, Reynoud N, Lahaye M, Marion D, Bakan B, Rothan C. Unraveling cuticle formation, structure, and properties by using tomato genetic diversity. *Front Plant Sci.* 2021;12:778131. <https://doi.org/10.3389/fpls.2021.778131>.
- Philippe G, Gaillard C, Petit J, Geneix N, Dalgalarondo M, Bres C, et al. Ester-crosslink profiling of the cutin polymer of Wild-Type and cutin synthase tomato (*Solanum lycopersicum* L.) mutants highlights different mechanisms of polymerization. *Plant Physiol.* 2016;170:807–20. <https://doi.org/10.1104/pp.15.01620>.
- Philippe G, Geneix N, Petit J, Guillon F, Sandt C, Rothan C, et al. Assembly of tomato fruit cuticles: a cross-talk between the cutin polyester and cell wall polysaccharides. *New Phytol.* 2020;226:809–22. <https://doi.org/10.1111/nph.16402>.
- Philippe G, Sørensen I, Jiao C, Sun X, Fei Z, Domozych DS, Rose JK. Cutin and suberin: assembly and origins of specialized lipidic cell wall scaffolds. *Curr Opin Plant Biol.* 2020;55:11–20. <https://doi.org/10.1016/j.pbi.2020.01.008>.
- Reca IB, Lionetti V, Camardella L, D'Avino R, Giardina T, Cervone F, Bellincampi D. A functional pectin methylesterase inhibitor protein (SolyPMEI) is expressed during tomato fruit ripening and interacts with PME-1. *Plant Mol Biol.* 2012;79:429–42. <https://doi.org/10.1007/s11103-012-9921-2>.
- Renaudin JP, Deluche C, Cheniclet C, Chevalier C, Frangne N. Cell layer-specific patterns of cell division and cell expansion during fruit set and fruit growth in tomato pericarp. *J Exp Bot.* 2017;68:1613–23. <https://doi.org/10.1093/jxb/erx058>.
- Reynoud N, Petit J, Bres C, Lahaye M, Rothan C, Marion D, Bakan B. The complex architecture of plant cuticles and its relation to multiple biological functions. *Front Plant Sci.* 2021;12:782773. <https://doi.org/10.3389/fpls.2021.782773>.
- Rose JKC, Braam J, Fry SC, Nishitani K. The XTH family of enzymes involved in xyloglucan endotransglucosylation and endohydrolysis: current perspectives and a new unifying nomenclature. *Plant Cell Physiol.* 2002;43:1421–35. <https://doi.org/10.1093/pccp/pcf171>.
- Rothan C, Just D, Fernandez L, Atienza I, Ballias P, Lemaire-Chamley M. Culture of the tomato Micro-Tom cultivar in greenhouse. *Methods Mol Biol.* 2016;1363:57–64. https://doi.org/10.1007/978-1-4939-3115-6_6.
- Sarnowska E, Gratkowska DM, Sacharowski SP, Cwiek P, Tohge T, Fernie AR, et al. The role of SWI/SNF chromatin remodeling complexes in hormone crosstalk. *Trends Plant Sci.* 2016;21:594–608. <https://doi.org/10.1016/j.tplants.2016.01.017>.
- Segado P, Heredia-Guerrero JA, Heredia A, Domínguez E. Cutinsomes and CUTIN SYNTHASE1 function sequentially in tomato fruit cutin deposition. *Plant Physiol.* 2020;183:1622–37. <https://doi.org/10.1104/pp.20.00516>.
- Shi JX, Malitsky S, De Oliveira S, Branigan C, Franke RB, Schreiber L, Aharoni A. SHINE transcription factors act redundantly to pattern the archetypal surface of *Arabidopsis* flower organs. *PLoS Genet.* 2011;7:e1001388. <https://doi.org/10.1371/journal.pgen.1001388>.
- Shi JX, Adato A, Alkan N, He Y, Lashbrooke J, Matas AJ, et al. The tomato SISHINE3 transcription factor regulates fruit cuticle formation and epidermal patterning. *New Phytol.* 2013;197:468–80. <https://doi.org/10.1111/nph.12032>.
- Shinozaki Y, Nicolas P, Fernandez-Pozo N, Ma Q, Evanich DJ, Shi Y, et al. High-resolution spatiotemporal transcriptome mapping of tomato fruit development and ripening. *Nat Commun.* 2018;9:364. <https://doi.org/10.1038/s41467-017-02782-9>.
- Shirasawa K, Hirakawa H, Nunome T, Tabata S, Isoe S. Genome-wide survey of artificial mutations induced by ethyl methanesulfonate and gamma rays in tomato. *Plant Biotechnol J.* 2016;14:51–60. <https://doi.org/10.1111/pbi.12348>.
- Smith DL, Gross KC. A family of at least seven beta-galactosidase genes is expressed during tomato fruit development. *Plant Physiol.* 2000;123:1173–83. <https://doi.org/10.1104/pp.123.3.1173>.
- Smith SM, Maughan PJ. SNP genotyping using KASPar assays. *Methods Mol Biol.* 2015;1245:243–56. https://doi.org/10.1007/978-1-4939-1966-6_18.
- Song X, Xu L, Yu J, Tian P, Hu X, Wang Q, Pan Y. Genome-wide characterization of the cellulose synthase gene superfamily in *Solanum lycopersicum*. *Gene.* 2019;688:71–83. <https://doi.org/10.1016/j.gene.2018.11.039>.
- Sousa AO, Camillo LR, Assis ETCM, Lima NS, Silva GO, Kirch RP, et al. EgPHI-1, a PHOSPHATE-INDUCED-1 gene from *Eucalyptus globulus*, is involved in shoot growth, xylem fiber length and secondary cell wall properties. *Planta.* 2020;252:45. <https://doi.org/10.1007/s00425-020-03450-x>.
- Tanaka T, Tanaka H, Machida C, Watanabe M, Machida Y. A new method for rapid visualization of defects in leaf cuticle reveals five intrinsic patterns of surface defects in *Arabidopsis*. *Plant J.* 2004;37:139–46. <https://doi.org/10.1046/j.1365-3113x.2003.01946.x>.
- Tomato Genome Consortium. The tomato genome sequence provides insights into fleshy fruit evolution. *Nature.* 2012;485:635–41. <https://doi.org/10.1038/nature11119>.
- Voisin D, Nawrath C, Kurdyukov S, Franke RB, Reina-Pinto JJ, Efreanova N, et al. Dissection of the complex phenotype in cuticular mutants of *Arabidopsis* reveals a role of SERRATE as a mediator. *PLoS Genet.* 2009;10:e1000703. <https://doi.org/10.1371/journal.pgen.1000703>.
- Xiong C, Xie Q, Yang Q, Sun P, Gao S, Li H, et al. WOOLLY, interacting with MYB transcription factor MYB31, regulates cuticular wax biosynthesis by modulating CER6 expression in tomato. *Plant J.* 2020;103:323–37. <https://doi.org/10.1111/tpj.14733>.
- Xu B, Taylor L, Pucker B, Feng T, Glover BJ, Brockington SF. The land plant-specific MIXTA-MYB lineage is implicated in the early evolution of the plant cuticle and the colonization of land. *New Phytol.* 2020;229:2324–38. <https://doi.org/10.1111/nph.16997>.
- Yeats TH, Rose JKC. The biochemistry and biology of extracellular plant lipid-transfer proteins (LTPs). *Protein Sci.* 2008;17:191–8. <https://doi.org/10.1110/ps.073300108>.
- Yeats TH, Martin LB, Viart HM, Isaacson T, He Y, Zhao L, et al. The identification of cutin synthase: formation of the plant polyester cutin. *Nat Chem Biol.* 2012;8:609–11. <https://doi.org/10.1038/nchembio.960>.
- Blast2GO. <https://www.blast2go.com/>. Accessed 11 Oct 2021.
- SGN (Sol Genomics Network). <https://solgenomics.net>. Accessed 11 Oct 2021.
- TAIR (The Arabidopsis Information Resource). <https://www.arabidopsis.org>. Accessed 11 Oct 2021.
- Tamura K, Stecher G, and Kumar S 2021. MEGA11: Molecular Evolutionary Genetics Analysis version 11 (<https://doi.org/10.1093/molbev/msab120>)

Publisher's Note

Springer Nature remains neutral with regard to jurisdictional claims in published maps and institutional affiliations.